Available online at www.sciencedirect.com
SCIENCE DIRECT
International Journal of Fatigue 27 (2005) 1277–1296
International Journal of Fatigue
www.elsevier.com/locate/ijfatigue

A two parameter driving force for fatigue crack growth analysis

A.H. Noroozi, G. Glinka*, S. Lambert

Department of Mechanical Engineering, University of Waterloo, Waterloo, Ont., Canada N2L 3G1

Available online 31 August 2005

Abstract

A model for fatigue crack growth (FCG) analysis based on the elastic–plastic crack tip stress–strain history was proposed. The fatigue crack growth was predicted by simulating the stress–strain response in the material volume adjacent to the crack tip and estimating the accumulated fatigue damage. The fatigue crack growth was regarded as a process of successive crack re-initiation in the crack tip region. The model was developed to predict the effect of the mean stress including the influence of the applied compressive stress. A fatigue crack growth expression was derived using both the plane strain and plane stress state assumption. It was found that the FCG was controlled by a two parameter driving force in the form of: $\Delta\kappa = K^{p}_{\max,\mathrm{tot}}\Delta K^{(1-p)}_{\mathrm{tot}}$. The driving force was derived on the basis of the local stresses and strains at the crack tip using the Smith–Watson–Topper (SWT) fatigue damage parameter: $D=\sigma_{\max}\Delta\varepsilon/2$.The effect of the internal (residual) stress induced by the reversed cyclic plasticity was accounted for the subsequent analysis. Experimental fatigue crack growth data sets for two aluminum alloys (7075-T6 and 2024-T351) and one steel alloy (4340) were used for the verification of the model.

Keywords: Driving force; Fatigue crack growth; Residual stress; R-ratio effects

1. Introduction

The first fatigue crack propagation expression (1) formulated in terms of the stress intensity factor was proposed by Paris and Erdogan [1]:

$$\frac{\mathrm{d}a}{\mathrm{d}N} = C(\Delta K_{\mathrm{appl}})^{m} \tag{1}$$

The Paris fatigue Eq. (1) prompted widely spread research activities aiming at possible improvements of its original form and at analytical modeling of FCG in general. One of the first problems concerning expression (1) and all other fatigue damage accumulation models is the quantification of the mean stress effect represented by the mean stress intensity factor in the case of fatigue crack growth analyses.

Elber [2] was the first one who suggested quantifying the mean stress effect on fatigue crack growth by using the concept of the crack tip closure. Numerous fatigue crack propagation models [3,4] based on that concept were proposed following Elber's ideas. The most popular among them is the semi-empirical fatigue crack propagation model developed by Newman [5]. Unfortunately, the crack tip closure model, in spite of the fact that it has been applied in the aircraft industry, is not easy to use and requires some experimental calibration. The contemporary belief is that the crack tip closure concept can explain both the mean stress and the variable amplitude effect on the fatigue crack growth.

An early empirical and relatively successful fatigue crack growth model accounting for the mean stress effect was proposed by Walker [6].

$$\frac{\mathrm{d}a}{\mathrm{d}N} = C[(1-R)^{P}K_{\max,\mathrm{appl}}]^{\gamma} = C[\Delta K^{(1-p)}_{\mathrm{appl}}K^{p}_{\max,\mathrm{appl}}]^{\gamma} \tag{2}$$

A similar expression was proposed later by Donald and Paris [7]. In both cases, expression (2) was capable to correlate fatigue crack growth rates obtained at a variety of relatively high stress ratios $R>0.4$. Unfortunately, it was not clearly indicated how the fatigue crack growth data for stress ratios $R<0$ should be correlated by expression (2).

Kujawski [8] proposed an analogous formula to expression (2) but including only the tensile part of

* Corresponding author. Tel.: +1 519 888 4567x3339; fax: +1 519 888 6197.
E-mail address: gggreg@mecheng1.uwaterloo.ca (G. Glinka).

0142-1123/$ - see front matter © 2005 Elsevier Ltd. All rights reserved.
doi:10.1016/j.ijfatigue.2005.07.002

Nomenclature

a	crack length
b	fatigue strength exponent
c	fatigue ductility exponent
C	fatigue crack growth constant
C^*	fatigue crack growth equation constant for plane strain
$\mathrm{d}a/\mathrm{d}N$	crack growth rate
D	fatigue damage
E	modulus of elasticity
FCG	fatigue crack growth
$f(\sigma^{\mathrm{a}}_{\mathrm{eq}})$	plastic strain expression (function)
K	stress intensity factor
K'	cyclic strength coefficient
$K_{\mathrm{max,appl}}$	maximum applied stress intensity factor
$K_{\mathrm{max,th}}$	maximum threshold stress intensity factor
$K_{\mathrm{max,tot}}$	total maximum stress intensity factor
$K_{\mathrm{min,appl}}$	minimum applied stress intensity factor
$K_{\mathrm{max,net}}$	maximum net stress intensity factor
$K_{\mathrm{min,net}}$	minimum net stress intensity factor
K_{net}	net stress intensity factor
$K_{\mathrm{min,tot}}$	total minimum stress intensity factor
K_{r}	residual stress intensity factor
ΔK_{appl}	applied stress intensity range
ΔK^{+}	tensile part of the stress intensity range
ΔK_{net}	net stress intensity range
ΔK_{th}	threshold stress intensity range
ΔK_{tot}	total stress intensity range
$\Delta\kappa$	two parameter driving force
m	Paris' equation exponent
$m(x,a)$	weight function
M_1, M_2, M_3	weight function parameters
N	number of cycle
N_{f}	number of cycle to fail the first element
n'	cyclic strain hardening exponent
p	driving force constant
r	radial polar coordinate
r_{p}	plastic zone size
R	stress ratio
R_{appl}	applied stress ratio
SIF	stress intensity factor
$S_{\mathrm{max,appl}}$	maximum applied nominal (remote) stress
$S_{\mathrm{min,appl}}$	minimum applied nominal (remote) stress
SWT	Smith–Watson–Topper fatigue damage parameter
x	distance from the crack tip
Y	geometrical stress intensity correction factor
ε	strain
$\varepsilon'_{\mathrm{f}}$	fatigue ductility coefficient
$\tilde{\varepsilon}^{\mathrm{a}}_{\mathrm{m}}$	maximum actual strain over the first elementary block
$\tilde{\varepsilon}^{\mathrm{e}}_{i}$	average elastic strain over the ith elementary material block
$\tilde{\varepsilon}^{\mathrm{a}}_{i}$	average actual strain over the ith elementary material block
$\Delta\varepsilon$	strain range ahead of the crack tip
$\Delta\tilde{\varepsilon}^{\mathrm{a}}$	actual strain range over the first elementary block
γ	fatigue crack growth equation exponent
ρ^*	notch tip radius or elementary material block size
ν	Poisson's coefficient
σ	stress
σ'_{f}	fatigue strength coefficient
σ_{max}	maximum stress ahead of the crack tip
$\tilde{\sigma}^{\mathrm{a}}_{\mathrm{max,th}}$	actual maximum threshold stress over the first elementary block
σ_x, σ_y, τ_{xy}	stress components
$\tilde{\sigma}^{\mathrm{a}}_{i}$	average actual stress over the ith elementary block
$\tilde{\sigma}^{\mathrm{a}}_{\mathrm{eq}}$	equivalent actual stress
$\tilde{\sigma}^{\mathrm{a}}_{\mathrm{m}}$	mean actual stress over the first elementary block
$\tilde{\sigma}^{\mathrm{e}}_{i}$	average pseudo-elastic stress over the ith elementary block
$\tilde{\sigma}^{\mathrm{e}}_{\mathrm{max,net}}$	maximum net pseudo-elastic stress over the first elementary block
$\tilde{\sigma}^{\mathrm{e}}_{\mathrm{min,net}}$	minimum net pseudo-elastic stress over the first elementary block
$\sigma^{e}_{\mathrm{min,net}}$	minimum net pseudo-elastic stress at the crack tip
σ_{r}	residual stress
$\Delta\tilde{\sigma}^{\mathrm{a}}$	actual stress range over the first elementary block
$\Delta\tilde{\sigma}^{\mathrm{e}}_{\mathrm{net}}$	net elastic stress range over the first elementary block
$\Delta\sigma_{\mathrm{th}}$	threshold stress range
$\Delta\tilde{\sigma}^{\mathrm{a}}_{\mathrm{th}}$	actual threshold stress range over the first elementary block
$\pi = 3.14$	constant
ψ_i	the averaging constant corresponding to the ith elementary block

the load cycle, i.e. the tensile part of the stress intensity range ΔK^{+}.

$$\frac{\mathrm{d}a}{\mathrm{d}N} = C[(\Delta K^{+})^{(1-p)}K^{p}_{\mathrm{max,appl}}]^{\gamma} \tag{3}$$

It was shown [8] that by empirical fitting of parameters p and γ it was possible to correlate fatigue crack growth data for stress ratios in the range of $1 \leq R < -1$. However, the correlation of experimental data for positive stress ratios $1 \leq R \leq 0$ was better than for negative ones $-1 < R < 0$.

A two parameter driving force involving the maximum stress intensity factor, K_{max} and the stress intensity range, ΔK was also suggested by Sadananda and Vasudevan [9]. In addition, they postulated the existence of two thresholds, i.e. the maximum threshold stress intensity factor $K_{max,th}$ and the threshold stress intensity range ΔK_{th}. Both should simultaneously be exceeded to make the fatigue crack grow.

In order to account for the mean stress effect, a fatigue crack growth model based on the analysis of the elastic–plastic strain–stress history at the crack tip is proposed below. The purpose of the model is to derive a fatigue crack model accounting for the mean stress and for the variable amplitude loading history effects by simulating the elastic–plastic response of the material in the crack tip region.

2. The fatigue crack propagation model

It is generally accepted that the local stresses and strains near the crack tip control the fatigue crack growth process. Unfortunately, the determination of the crack tip stress and strain in the case of elastic–plastic behavior is difficult and strongly dependent on the theoretical and numerical method used for the analysis. Therefore, fracture mechanics principles are often used in order to defocus the attention from the local crack tip stress–strain field and to express all necessary quantities in terms of global parameters such as the nominal stress, crack size, and geometry, etc. combined into one parameter called the stress intensity factor (SIF). Such approaches are successful as long as the SIF is uniquely correlated with the actual elastic–plastic crack tip stress–strain field. Unfortunately, the correlation between the SIF and the crack tip stress–strain filed is often altered by residual stresses induced by reversed plastic deformations.

There are several difficulties in defining the crack tip geometry on the basis of the mechanics of continuum. The classical fracture mechanics solutions [10,11] concerning stresses and strains at the crack tip were derived for a sharp crack having the tip radius $\rho^*=0$. Such crack tip geometry leads to a singular solution resulting in unrealistically high strains and stresses in the vicinity of the crack tip. In spite of the importance of these fundamental fracture mechanics solutions, they cannot be used for the determination of the actual stresses and strains in the vicinity of the crack tip. Therefore, several attempts were made in the past [12–14] to model the crack as a notch with a small but finite tip radius $\rho^*>0$. The advantage of using the blunt crack model lies in the fact that the notch theories can be applied and the calculated crack tip stresses and strains become more realistic. There are two important implications resulting from such a model, i.e. the crack tip radius is assumed to be finite ($\rho^*>0$) and the crack region just behind the tip (Fig. 1) remains open.

In the case of pure elastic behavior, the crack subjected to tensile loading behaves like a notch of length/depth $2a$ with the tip radius equal to ρ^*. However, under compressive loading, the opposite crack surfaces come in to contact with each other except the region just behind the crack tip. In the latest configuration (Fig. 1(b)), the crack induces the same local stress field as two circular notches under compressive loading. The argument for assuming such a crack model comes from the Neuber micro-support concept [15] used for calculating the fatigue notch factor. Neuber suggested that

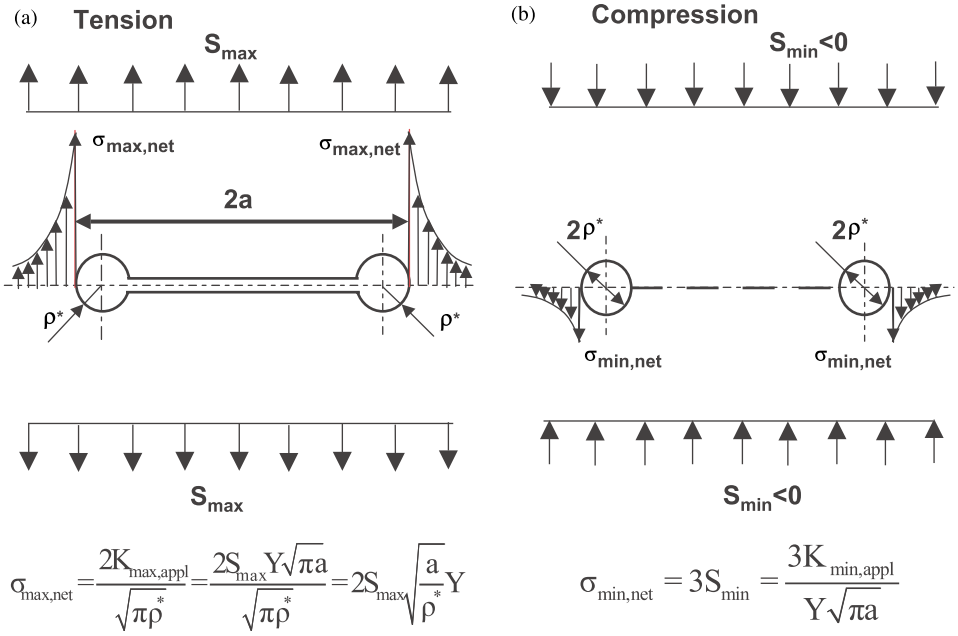

Fig. 1. A crack model for linear-elastic analysis of stresses and strains near the crack tip: (a) stress concentration near the crack tip according to Creager–Paris solution; (b) stress concentration for a circular notch simulating the crack under compressive loading.

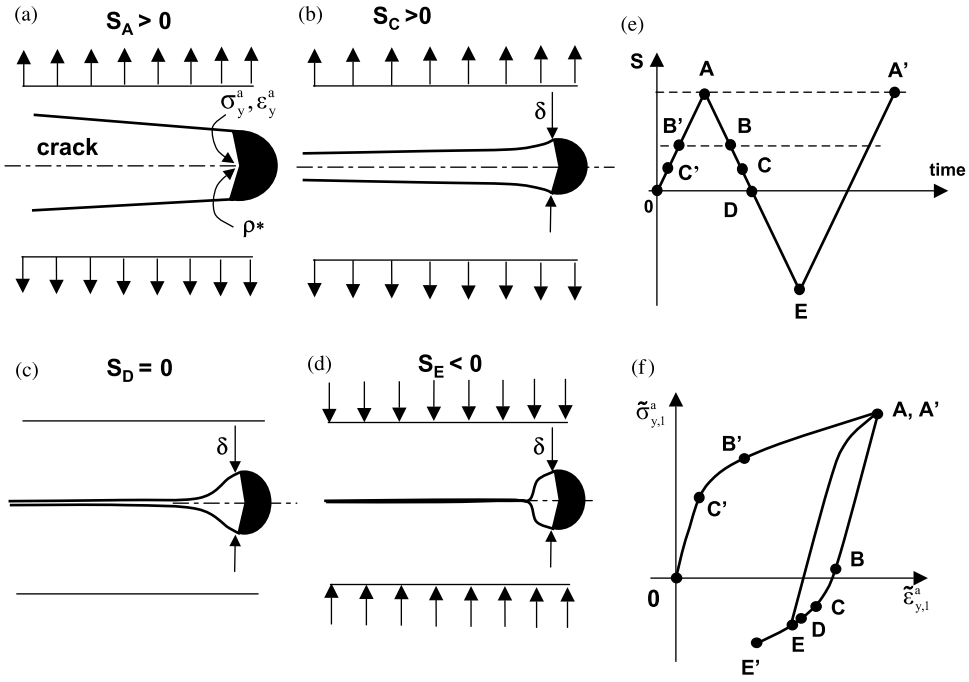

Fig. 2. Approximate crack tip geometry, the cyclic plastic zone and the crack tip stress–strain response: (a)–(d) evolution of the crack opening displacements in the crack region; (e) applied load (stress intensity factor) history; (f) qualitative stress–strain response at the crack tip.

there is a limit concerning the smallest notch tip radius material can 'feel' as a notch. The minimum effective notch tip radius ρ^* was considered to be a material property determining the maximum stress concentration which can be generated in the material.

In the case of plastic yielding around the crack tip due to the Bauschinger effect, the plastic deformations induced by the first reversal of cyclic loading are greater than those generated during subsequent unloading reversal even if both reversals have the same magnitude. The plastically deformed material volume near the crack tip resists to be deformed during subsequent reversals of cyclic loading. Therefore, the cyclic deformations near a tip of propagating fatigue crack may be smaller than the deformations induced during the first reversal of loading. For this reason, the region just behind the crack tip may stay open even under the compressive minimum load. In other words, the cyclic plastic zone ahead of the crack tip, created by the first two reversals, can be considered as an obstacle (Fig. 2(a)–(d)) resisting to be deformed during subsequent stress/load reversals. The plastic zone at the crack tip created by first two reversals may also be considered as a small 'ball' which resists being deformed during the following load reversals. Schematically this effect is illustrated in Fig. 2(e) and (f) showing the applied load history and qualitative variations of the stress and strain at the crack tip. The plastic deformations are induced during the first nominal stress/load reversal from 0 to A (Fig. 2(a)). During the unloading reversal, due to the increase of the yield limit (Bauschinger effect) and the subsequent increase of the deformational stiffness of the plastic zone (Fig. 2(e) and (f)) the reversed plastic deformations begin at the load level C and the effectiveness of the remaining part of the unloading reversal decreases. Therefore, the crack tip stress and strain path ends at point E (Fig. 2(f)) instead of point E′, which would be attained if the plastic zone did not resist deformation. A very small or non-existent change of the opening displacement behind the crack tip during the load excursion from level C to E can be interpreted, based on global macro-measurements such as the crack tip closure even if there is no physical contact between crack surfaces. The consequences are that small cyclic fluctuations of the crack opening displacement behind the crack tip result in small strain fluctuations in the material ahead of the crack tip. The possibility of the existence of the 'empty' or the stress free space behind the crack tip was found experimentally by Jones [16]. The 'empty' stress free region appearing just behind the crack tip was also found by carrying out very thorough Finite Element analyses [17,18]. The plastic zone effect on the displacements behind the crack tip can be modeled by assuming the displacements field around the crack tip in the form of an opening shown in Fig. 3(a). From the superposition point of view, the plastic zone deformations and the displacement field behind the crack tip, shown in Fig. 3(a), can be replaced by the equivalent stress field as shown in Fig. 3(b). Such a stress field is qualitatively similar to the stress field generated by a pile of dislocations activated in the crack tip region. It is assumed that the residual stress $\sigma_r(x)$ in the plastic zone is generated by reversed plastic deformations ahead of the crack tip and can be determined by solving the elastic–plastic notched body boundary problem. A symmetric compressive residual stress

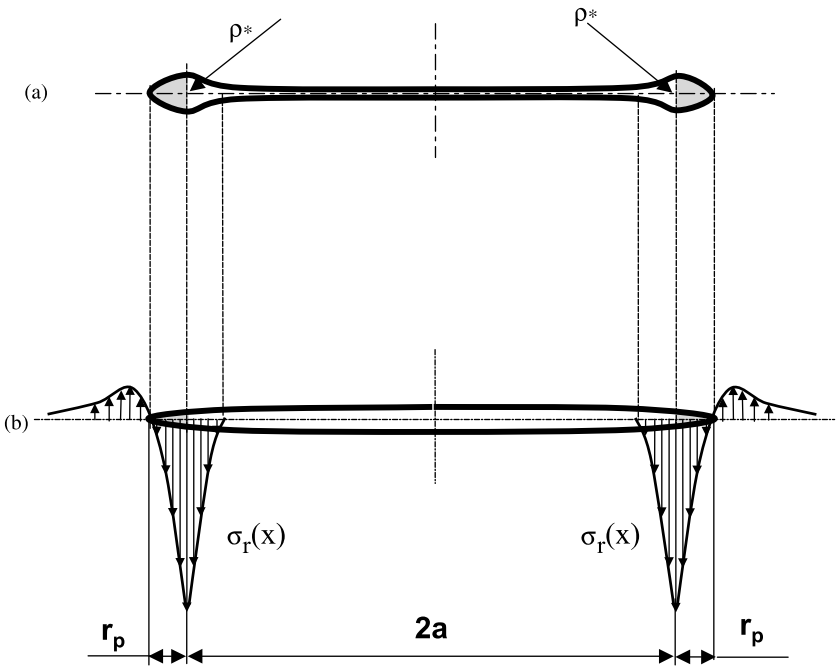

Fig. 3. Approximate crack tip displacement field and corresponding residual stress distributions: (a) illustration of the displacement field around the plastic zone; (b) the residual stress distribution required for generating the displacement field.

field is added in order to simulate the effect of the opening behind the physical crack tip. The resultant model of the crack tip region, accounting for the plastic zone deformational resistance and the opening behind the crack tip, is shown in Fig. 3(b). Thus, the effect of the plastic zone and the crack tip opening behind the crack tip can be subsequently quantified by estimating the residual stress contribution to the magnitude of the applied stress intensity range. Two effects need to be considered, i.e. the difference in the stress/strain concentration at the crack tip associated with the tensile and compressive part of the loading cycle (Fig. 1), and secondly the effect of the plasticity induced residual stresses around the crack tip.

A real engineering material according to the Neuber micro-support concept [15] can be modeled (Fig. 4) as a medium made of elementary blocks of dimension ρ^*. The elementary material block can be considered as the smallest material volume to which the mechanics of continuum and bulk material properties such as modulus of elasticity E, Poisson's ratio ν, the strength coefficient K' and the strain hardening exponent n' can be applied. The same idea, but from the material science point of view was also discussed by

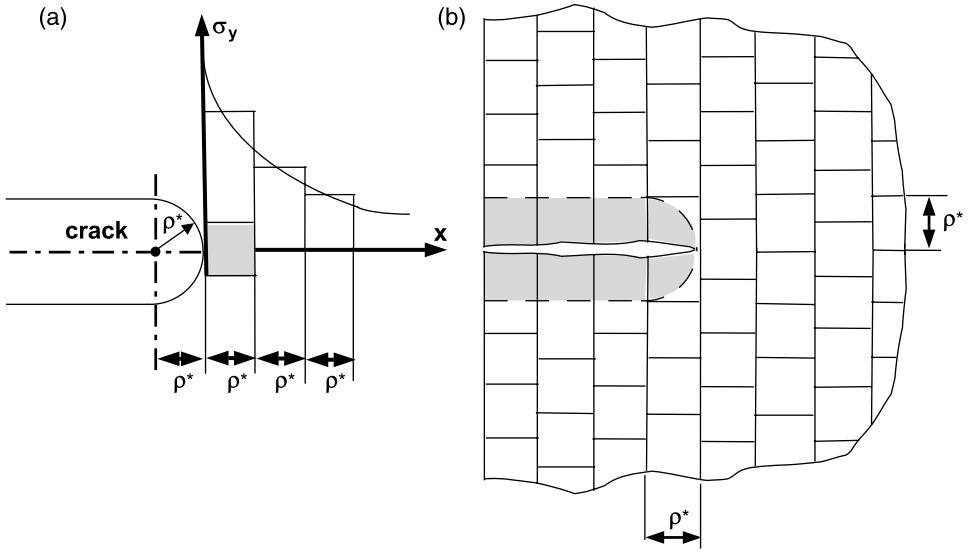

Fig. 4. The idealized crack tip geometry and the discrete structure of a material: (a) the crack tip geometry and averaged stresses over individual elementary material blocks; (b) a crack and the discrete elementary material blocks.

Forsyth [19]. Forsyth [19] stated that "the micro-structural features in metals cause the break up of the crack front into segments that relate to elementary blocks operating with some degree of independence from their neighbors but under the general influence of the macroscopic crack of which they are part". Therefore, it is anticipated that the dimension ρ^* can be indirectly dependent on the micro-structural features of the analyzed material, but it cannot be uniquely associated with any specific micro-structural particle size. The elementary material block size ρ^* can be understood rather as an average dimension of inhomogeneous material blocks which still behave like the bulk material of a larger volume. The resolution of the mechanics of continuum is not sufficient to determine the meaningful stress and strain field within the elementary blocks of size ρ^*. Therefore, only the average continuum mechanics stresses and strains can be assigned to the elementary blocks of a material.

Based on the observations discussed above, the following fatigue crack model is proposed.

- The material is assumed to be composed of identical elementary material blocks of a finite linear dimension ρ^* (Fig. 4).
- The fatigue crack can be analyzed as a notch with the tip radius ρ^*.
- The fatigue crack growth is regarded as successive crack re-initiations over the distance ρ^*.
- The material properties used in the proposed model are the Ramberg–Osgood cyclic stress strain curve [20]

$$\varepsilon = \frac{\sigma}{E} + \left(\frac{\sigma}{K\prime}\right)^{1/n'} \tag{4}$$

and the strain–life (Manson–Coffin) fatigue curve [21].

$$\frac{\Delta\varepsilon}{2} = \frac{\sigma'_{\mathrm{f}}}{E}(2N)^b + \varepsilon'_{\mathrm{f}}(2N)^c \tag{5}$$

- The number of cycles N to failure of the first elementary block of the material at the crack tip can be determined from the strain–life (Manson–Coffin) fatigue curve (5) by accounting for the stress–strain history and using the Smith–Watson–Topper (SWT) fatigue damage parameter [22].

$$D = \sigma_{\max}\frac{\Delta\varepsilon}{2} \tag{6}$$

- The fatigue crack growth rate can be determined as the average fatigue crack propagation rate over the elementary material block of the size ρ^*.

$$\frac{\mathrm{d}a}{\mathrm{d}N} = \frac{\rho^*}{N} \tag{7}$$

The simulation of the crack tip stress–strain history includes the effect of the cyclic elastic–plastic stress–strain material behavior and the effect of the local residual stresses induced by the reversed cyclic plastic deformations in the crack tip region.

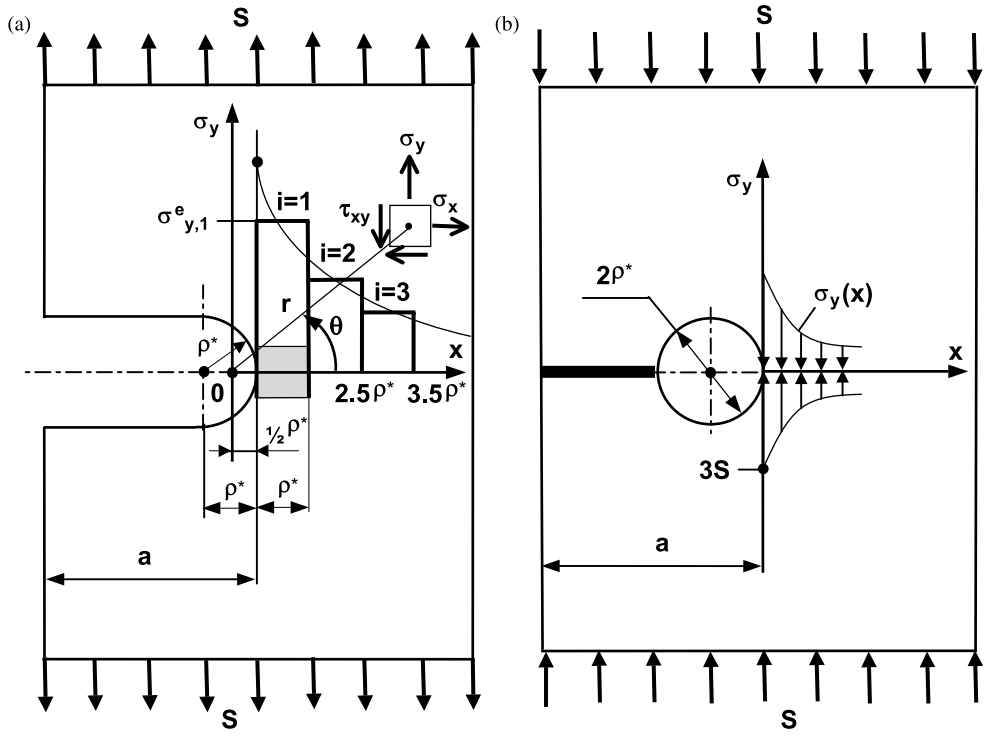

Fig. 5. Schematic of the stress distributions ahead of the crack tip induced by a tensile and a compressive load: (a) stress concentration and the nomenclature for the Creager–Paris notch tip stress expressions; (b) stress concentration and stress distribution induced by compressive loading.

3. Analysis of strains and stresses at the crack tip

The calculation of elastic–plastic strains and stresses at the crack tip requires the solving of the elastic–plastic boundary problem of a cracked body. Analytical solutions of such complex problems are seldom attainable. Numerical solutions using the Finite Element method are feasible but not very convenient in practice due to the complexity of FE models and lengthy in the case of cyclic loading calculations. Therefore, a simplified method based on the Neuber rule [23] was applied. The method requires a two-step approach, i.e. first the linear-elastic stress–strain analysis needs to be carried out and in the second step the actual elastic–plastic crack tip strains and stresses are determined from the Neuber rule, for which the linear-elastic stress data is the input.

3.1. Linear-elastic analysis of stresses and strains near the blunt crack tip

The fatigue crack growth expressions are frequently formulated in terms of the stress intensity factor, K. Therefore, the analysis below is also carried out using the stress intensity factor and fracture mechanics principles, wherever possible. The linear-elastic stress–strain analysis must also be carried out using a two-step approach because the stress response at the crack tip to the tensile load, no contact between crack surfaces, is different from the compressive one.

3.1.1. Crack tip stresses induced by tensile loading ($K_{min,appl}>0$)

The calculations of linear-elastic stresses and strains induced by tensile loading are in essence reduced to the analysis of a notch of depth 'a' having a tip radius ρ^* (Fig. 5(a)).

The Creager–Paris solution [24] was used assuming the crack tip radius ρ^* would be small in comparison with the crack depth 'a'

$$\sigma_x = -\frac{K}{\sqrt{2\pi r}}\frac{\rho^*}{2r}\cos\frac{3\theta}{2} + \frac{K}{\sqrt{2\pi r}}\cos\frac{\theta}{2}\left[1-\sin\frac{\theta}{2}\sin\frac{3\theta}{2}\right]+\cdots \tag{8a}$$

$$\sigma_y = \frac{K}{\sqrt{2\pi r}}\frac{\rho^*}{2r}\cos\frac{3\theta}{2} + \frac{K}{\sqrt{2\pi r}}\cos\frac{\theta}{2}\left[1+\sin\frac{\theta}{2}\sin\frac{3\theta}{2}\right]+\cdots \tag{8b}$$

$$\tau_{xy} = -\frac{K}{\sqrt{2\pi r}}\frac{\rho^*}{2r}\sin\frac{3\theta}{2} + \frac{K}{\sqrt{2\pi r}}\sin\frac{\theta}{2}\cos\frac{\theta}{2}\cos\frac{3\theta}{2} + \cdots \tag{8c}$$

The linear-elastic stress components along the crack plane ($\theta=0$, $r=x$) are:

$$\sigma_x = \frac{K}{\sqrt{2\pi x}}\left(1-\frac{\rho^*}{2x}\right)+\cdots \tag{9a}$$

$$\sigma_y = \frac{K}{\sqrt{2\pi x}}\left(1+\frac{\rho^*}{2x}\right)+\cdots \tag{9b}$$

$$\tau_{xy} = 0 \tag{9c}$$

The maximum stress at the crack tip can be determined from the applied stress intensity factor, assuming $x=\rho^*/2$.

$$\sigma_y = \frac{2K}{\sqrt{\pi\rho^*}} \tag{10}$$

However, the calculations need to be carried out for elementary material blocks with the size ρ^*. Therefore, the average stress over each elementary block was used in the analysis.

$$\tilde{\sigma}^{e}_{y,i} = \frac{1}{x_{i+1}-x_i}\int_{x_i}^{x_{i+1}}\frac{K}{\sqrt{2\pi x}}\left(\frac{\rho^*}{2x}+1\right)\mathrm{d}x \tag{11}$$

After integrating expression (11), the average stress over the elementary block i can be written in the form:

$$\tilde{\sigma}^{e}_{y,i} = \frac{K\times\psi_{y,i}}{\sqrt{2\pi\rho^*}} \tag{12}$$

where $\psi_{y,1}=1.633$, $\psi_{y,2}=0.8967$, $\psi_{y,3}=0.6773$, $\psi_{y,4}=0.5641$.

A similar expression can be derived for the stress component σ_x.

$$\tilde{\sigma}^{e}_{x,i} = \frac{K\times\psi_{x,i}}{\sqrt{2\pi\rho^*}} \tag{13}$$

where $\psi_{x,1}=0.4376$, $\psi_{x,2}=0.5287$, $\psi_{x,3}=0.4814$, $\psi_{x,4}=0.4378$.

Based on Eq. (12), the maximum and minimum linear-elastic stresses and the stress range over the first elementary material block induced by the applied maximum nominal tensile stress $S_{max,appl}>0$ (or the maximum stress intensity factor $K_{max,appl}$) and the applied minimum tensile stress $S_{min,appl}>0$ can be calculated as:

$$\tilde{\sigma}^{e}_{max,net} = \frac{\psi_{y,1}K_{max,appl}}{\sqrt{2\pi\rho^*}} = \frac{\psi_{y,1}S_{max,appl}Y\sqrt{\pi a}}{\sqrt{2\pi\rho^*}} = S_{max,appl}Y\sqrt{\frac{a}{2\rho^*}}\psi_{y,1} \tag{14}$$

$$\tilde{\sigma}^{e}_{min,net} = \frac{\psi_{y,1}K_{min,appl}}{\sqrt{2\pi\rho^*}} = \frac{\psi_{y,1}S_{min,appl}Y\sqrt{\pi a}}{\sqrt{2\pi\rho^*}} = S_{min,appl}Y\sqrt{\frac{a}{2\rho^*}}\psi_{y,1} \tag{15}$$

$$\Delta\tilde{\sigma}^{e}_{net} = \frac{\psi_{y,1}K_{max,appl}}{\sqrt{2\pi\rho^*}} - \frac{\psi_{y,1}K_{min,appl}}{\sqrt{2\pi\rho^*}}$$

$$= \frac{\psi_{y,1}}{\sqrt{2\pi\rho^*}}\Delta K_{appl} = \Delta S_{appl} Y\sqrt{\frac{a}{2\rho^*}}\psi_{y,1} \quad (16)$$

where

$$S_{min,appl} = \frac{K_{min,appl}}{Y\sqrt{\pi a}}, \quad S_{max,appl} = \frac{K_{max,appl}}{Y\sqrt{\pi a}},$$

$$\Delta S_{appl} = \frac{\Delta K_{appl}}{Y\sqrt{\pi a}}$$

The nominal or reference stress ($S_{max,appl}$ or $S_{min,appl}$) in the stress intensity factor expression is easy to identify in the case of simple loading configuration such as uniform tension or bending. However, any stress magnitude can be chosen as a reference in the case of complex stress fields such as residual stress distributions or thermally induced stress fields. As long as the stress intensity factor is used as a load parameter, the choice of the reference stress is not important. Therefore, for consistency reasons the nominal stresses were defined as shown above.

Expressions (14)–(16) are valid only for tensile loading, i.e. for $K>0$ and the net stress components are needed as inputs into the Neuber equations.

3.1.2. Crack tip stresses induced by compressive loading ($K_{min,appl}<0$)

The crack tip stress concentration under compressive loading is much less than in tension. This is due to the fact that under the compressive minimum nominal stress, $S_{min,appl}<0$, the contact pressure is transferred through the contacting crack surfaces. In such a case, the crack should be treated, according to the model (Fig. 5(b)), as a single hole or two identical circular holes. The stress at the edge of a circular hole ($\theta=0$ and $x=\rho^*$) of diameter $2\rho^*$ in a wide plate can be estimated from the well-known classical solution [15] concerning the circular notch problem in an infinite plate ($\theta=0$ and $x=\rho^*$).

$$\sigma_x = S\left[1-2.5\left(\frac{\rho^*}{x}\right)^2 + 1.5\left(\frac{\rho^*}{x}\right)^4\right] \quad (17)$$

$$\sigma_y = S\left[1+0.5\left(\frac{\rho^*}{x}\right)^2 + 1.5\left(\frac{\rho^*}{x}\right)^4\right] \quad (18)$$

The stress concentration factor, according to Eq. (18), is 3 and the minimum compressive stress at the edge of the hole can be calculated as:

$$\sigma^{e}_{min,net} = 3S_{min,appl} \quad (19)$$

The applied nominal minimum stress, $S_{min,appl}$ can also be related to the minimum applied stress intensity factor:

$$S_{min,appl} = \frac{K_{min,appl}}{Y\sqrt{\pi a}} \quad (20)$$

Thus, the minimum local stress at the edge of a notch can finally be related to the minimum applied stress intensity factor, $K_{min,appl}$.

$$\sigma^{e}_{min,net} = \frac{3K_{min,appl}}{Y\sqrt{\pi a}} \quad (21)$$

However, the Creager–Paris solution (10) would suggest that if the problem is treated as a blunt crack, a certain net minimum stress intensity factor $K_{min,net}$ needs to be applied in order to generate the same stress at the crack tip as that one determined from Eq. (21).

$$\sigma^{e}_{min,net} = \frac{2K_{min,net}}{\sqrt{\pi\rho^*}} \quad (22)$$

Combination of Eqs. (21) and (22) makes it possible to determine the net stress intensity factor $K_{min,net}$ resulting in the same crack tip stress as that one calculated from Eq. (21) when substituted into the Creager–Paris expression (22).

$$K_{min,net} = K_{min,appl}\frac{3}{2Y}\sqrt{\frac{\rho^*}{a}} \quad \text{or}$$
$$\frac{K_{min,net}}{K_{min,appl}} = \frac{3}{2Y}\sqrt{\frac{\rho^*}{a}} \quad (23)$$

In order to determine fluctuations of the linear-elastic stress near the crack tip, it is necessary to account for the differences in the tensile and compressive part of the cycle, i.e.

$$\tilde{\sigma}^{e}_{max,net} = \frac{\psi_{y,1}K_{max,appl}}{\sqrt{2\pi\rho^*}} = \frac{\psi_{y,1}S_{max,appl}Y\sqrt{\pi a}}{\sqrt{2\pi\rho^*}}$$

$$= S_{max,appl}Y\sqrt{\frac{a}{2\rho^*}}\psi_{y,1} \quad (24)$$

$$\tilde{\sigma}^{e}_{min,net} = \frac{\psi_{y,1}K_{min,net}}{\sqrt{2\pi\rho^*}} = \frac{3\psi_{y,1}}{2\sqrt{2}}\frac{K_{min,appl}}{Y\sqrt{\pi a}}$$

$$= S_{min,appl}\frac{3\psi_{y,1}}{2\sqrt{2}} \quad (25)$$

$$\Delta\tilde{\sigma}^{e}_{net} = \tilde{\sigma}^{e}_{max,net} - \tilde{\sigma}^{e}_{min,net}$$

$$= \frac{\psi_{y,1}K_{max,appl}}{\sqrt{2\pi\rho^*}} - \frac{3\psi_{y,1}}{2\sqrt{2}}\frac{K_{min,appl}}{Y\sqrt{\pi a}}$$

$$= \frac{\psi_{y,1}}{\sqrt{2\pi\rho^*}}\left(K_{max,appl} - \frac{3}{2Y}\sqrt{\frac{\rho^*}{a}}K_{min,appl}\right) \quad (26)$$

It can be seen from Eq. (26) that the contribution of the compressive part of the applied stress reversal (from 0 to $K_{min,appl}$) to the local crack tip stress range is relatively small and it depends on the crack tip radius ρ^* and the crack size 'a'. It is possible that the circular whole approximation (Fig. 5(b)) might be non-conservative but this will be found later. The maximum crack tip stress $\tilde{\sigma}^{e}_{max,net}$ and the stress range $\Delta\tilde{\sigma}^{e}_{net}$ over the first elementary material block obtained

from the linear-elastic analysis are inputs for calculating the elastic–plastic stress–strain response.

3.2. Elastic–plastic analysis of stresses and strains near the crack tip

The purpose of the elastic–plastic stress–strain analysis is to determine the actual stress–strain history over the first ($i=1$) elementary material block and the residual stress induced by the reversed plastic yielding in the crack tip region.

To avoid solving the complete but unfortunately a very complex elastic–plastic cracked body boundary problem for each load/stress reversal, the well-known Neuber rule [23] was used. The Neuber rule was originally derived for a uni-axial stress state (i.e. pure shear) but it has been recently expanded for multi-axial proportional and non-proportional loading conditions [25,26]. The Neuber rule states the equivalence of the strain energy density at the notch tip between the linear-elastic and elastic–plastic behavior of geometrically identical notched bodies subjected to identical external loads. In the case of uni-axial stress state at the notch tip the Neuber rule provides the relationship between the hypothetical linear-elastic notch tip stress–strain input data and the actual elastic–plastic response.

$$\tilde{\sigma}^{e}_{y,i}\tilde{\varepsilon}^{e}_{y,i} = \tilde{\sigma}^{a}_{y,i}\tilde{\varepsilon}^{a}_{y,i} \tag{27}$$

For cracked bodies in plane stress the stress state near the crack tip is bi-axial. In the case of bodies in plane strain, the near tip stress state is tri-axial but the third principal stress is a function of the other two and in both situations the modified bi-axial Neuber rule [25] can be used. In addition, the elastic stress tensor used as the input does not rotate during loading and all stress components change proportionally. Therefore, the Hencky equations [27] of the total deformation theory of plasticity can be applied.

In the case of bi-axial stress state, the Hencky stress–strain relationships, the Ramberg–Osgood stress–strain constitutive Eq. (4) and the multi-axial Neuber rule [25] can be combined into the set of five equations. Using this set of equations, all elastic–plastic crack tip strains and stresses can be determined over each element ahead of the crack tip.

$$\begin{cases} \tilde{\varepsilon}^{a}_{x,i} = \dfrac{1}{E}(\tilde{\sigma}^{a}_{x,i} - \nu\tilde{\sigma}^{a}_{y,i}) + \dfrac{f(\sigma^{a}_{eq})}{\sigma^{a}_{eq}}\left(\tilde{\sigma}^{a}_{x,i} - \dfrac{1}{2}\tilde{\sigma}^{a}_{y,i}\right) \\ \tilde{\varepsilon}^{a}_{y,i} = \dfrac{1}{E}(\tilde{\sigma}^{a}_{y,i} - \nu\tilde{\sigma}^{a}_{x,i}) + \dfrac{f(\sigma^{a}_{eq})}{\sigma^{a}_{eq}}\left(\tilde{\sigma}^{a}_{y,i} - \dfrac{1}{2}\tilde{\sigma}^{a}_{x,i}\right) \\ \tilde{\varepsilon}^{a}_{z,i} = \dfrac{1}{E}[-\nu(\tilde{\sigma}^{a}_{x,i} + \tilde{\sigma}^{a}_{y,i})] + \dfrac{f(\sigma^{a}_{eq})}{\sigma^{a}_{eq}}\left[-\dfrac{1}{2}(\tilde{\sigma}^{a}_{x,i} + \tilde{\sigma}^{a}_{y,i})\right] \\ \tilde{\sigma}^{e}_{x,i}\tilde{\varepsilon}^{e}_{x,i} = \tilde{\sigma}^{a}_{x,i}\tilde{\varepsilon}^{a}_{x,i} \\ \tilde{\sigma}^{e}_{y,i}\tilde{\varepsilon}^{e}_{y,i} = \tilde{\sigma}^{a}_{y,i}\tilde{\varepsilon}^{a}_{y,i} \end{cases} \tag{28}$$

where

$$\sigma^{a}_{eq} = \sqrt{(\tilde{\sigma}^{a}_{x,i})^2 - \tilde{\sigma}^{a}_{x,i}\tilde{\sigma}^{a}_{y,i} + (\tilde{\sigma}^{a}_{y,i})^2} \quad \text{and}$$

$$f(\sigma^{a}_{eq}) = \left(\frac{\sigma^{a}_{eq}}{K'}\right)^{1/n'}$$

In the case of cracked bodies in plane stress, the stress state over the first elementary material block reduces to one normal stress component. Therefore, the equation set (28) reduces to the classical uni-axial Neuber rule associated with the Ramberg–Osgood equation.

$$\begin{cases} \tilde{\varepsilon}^{a}_{x,1} = -\dfrac{\nu}{E}\tilde{\sigma}^{a}_{y,1} - \dfrac{1}{2}\left(\dfrac{\tilde{\sigma}^{a}_{y,1}}{K'}\right)^{1/n'} \\ \tilde{\varepsilon}^{a}_{y,1} = \dfrac{\tilde{\sigma}^{a}_{y,1}}{E} + \left(\dfrac{\tilde{\sigma}^{a}_{y,1}}{K'}\right)^{1/n'} \\ \tilde{\varepsilon}^{a}_{z,1} = -\dfrac{\nu}{E}\tilde{\sigma}^{a}_{y,1} - \dfrac{1}{2}\left(\dfrac{\tilde{\sigma}^{a}_{y,1}}{K'}\right)^{1/n'} \\ \tilde{\sigma}^{e}_{y,1}\tilde{\varepsilon}^{e}_{y,1} = \tilde{\sigma}^{a}_{y,1}\tilde{\varepsilon}^{a}_{y,1} \end{cases} \tag{29}$$

The Neuber Eq. (27) can also be written in terms of the nominal stress or the stress intensity factor.

$$\tilde{\sigma}^{e}_{y,1}\tilde{\varepsilon}^{e}_{y,1} = \frac{(\tilde{\sigma}^{e}_{y,1})^2}{E} = \frac{1}{E}\left(\frac{\psi_{y,1}K_{net}}{\sqrt{2\pi\rho^*}}\right)^2 = \tilde{\sigma}^{a}_{y,1}\tilde{\varepsilon}^{a}_{y,1} \tag{30}$$

The maximum stress at the crack tip induced by the first reversal can be determined from the Neuber rule (30) and the Ramberg–Osgood strain–stress curve (4).

$$\begin{cases} \dfrac{1}{E}\left(\dfrac{K_{max,net}\times\psi_{y,1}}{\sqrt{2\pi\rho^*}}\right)^2 = \dfrac{(\tilde{\sigma}^{a}_{max})^2}{E} + \tilde{\sigma}^{a}_{max}\left(\dfrac{\tilde{\sigma}^{a}_{max}}{K'}\right)^{1/n'} \\ \tilde{\varepsilon}^{a}_{max} = \dfrac{\tilde{\sigma}^{a}_{max}}{E} + \left(\dfrac{\tilde{\sigma}^{a}_{max}}{K'}\right)^{1/n'} \end{cases} \tag{31}$$

The crack tip strain and stress ranges can be determined from the Neuber equation when written in terms of ranges and associated with the expanded by factor of two stress–strain curve.

$$\begin{cases} \dfrac{1}{E}\left(\dfrac{\Delta K_{net}\times\psi_{y,1}}{\sqrt{2\pi\rho^*}}\right)^2 = \dfrac{(\Delta\tilde{\sigma}^{a})^2}{E} + 2(\Delta\tilde{\sigma}^{a})\left(\dfrac{\Delta\tilde{\sigma}^{a}}{2K'}\right)^{1/n'} \\ \dfrac{\Delta\tilde{\varepsilon}^{a}}{2} = \dfrac{\Delta\tilde{\sigma}^{a}}{2E} + \left(\dfrac{\Delta\tilde{\sigma}^{a}}{2K'}\right)^{1/n'} \end{cases} \tag{32}$$

The equations above enable the determination of elastic–plastic strains and stresses at the crack tip induced by one

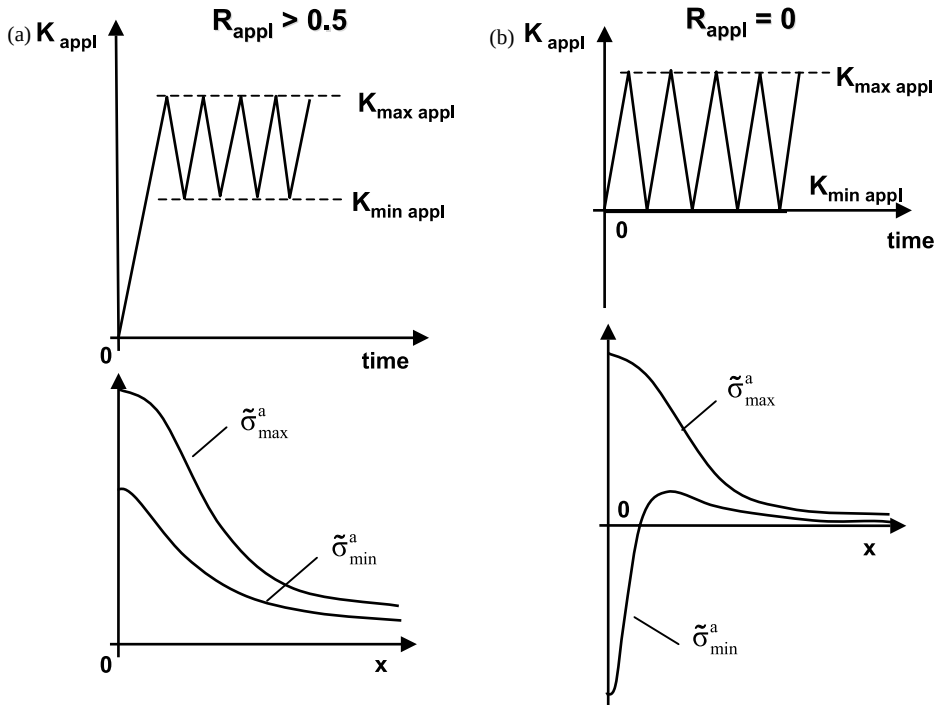

Fig. 6. Approximate elastic–plastic crack tip stress distribution induced by cyclic loading: (a) at high stress ratios $R>0.5$; (b) at low stress ratios $R\leq 0.5$.

reversal of the load history represented by the fluctuations of the stress intensity factor, ΔK_{net}. After calculating the actual elastic–plastic strains and stresses at various locations, the residual stress distribution $\sigma_r(x)$ induced by the application of the loading and unloading stress reversal can be determined.

Schematic diagrams in Fig. 6 show stress distributions ahead of the crack tip corresponding to the maximum and minimum load level at two different stress ratios R. Both stress distributions, i.e. those corresponding to the maximum and minimum load are most often tensile at high applied stress ratios ($R_{\text{appl}}>0.5$). In such a case, the crack tip displacement field and the crack tip stress field are dependent on the applied stress intensity factors only. However, compressive residual stresses might be generated at the minimum load level in the case of low stress ratios ($R_{\text{appl}}<0.5$). The residual stresses remain present in the crack tip region even at the zero applied load level. Therefore, the residual stresses have to be included into the relationship correlating the applied load, the crack tip stress–strain response and the displacement field. It is assumed that the compressive stress ahead of the crack tip is acting as a clamp over the crack tip region and its action has to be overcome before the increments of the applied (or the net) stress intensity range can be fully effective as stated in Eqs. (31) and (32). Again, the residual compressive stress effect needs to be expressed in terms of the stress intensity factor before it can be included in any fatigue crack growth expression.

The Neuber rule makes it possible to determine the residual stress distribution through the plastic zone but not behind the crack tip. However, in order to simulate the character of the displacement field around the crack tip, shown in Fig. 3(a), the compressive part of the residual stress field ahead of the crack tip was symmetrically added over the region behind the crack tip as shown in Fig. 3(b). The residual stress field shown in Fig. 3(b) was subsequently used for calculating the residual stress intensity factor, K_{r}.

3.3. Calculation of the residual stress intensity factor K_r

The compressive residual stress ahead of the crack tip prevents free deformation and opening displacement behind the crack tip. Therefore, it was assumed analogously to the well-known Dugdale [28] model, that the effect of residual stress $\sigma_{\text{r}}(x)$ could be expressed in terms of the stress intensity factor calculated for a crack (Fig. 3) tip surrounded by the compressive stress applied to the crack surface. The calculation of the residual stress intensity factor was carried out using the weight function method [29,30]. The universal weight function expression (33) was used in the analysis.

$$m(x,a)=\frac{2P}{\sqrt{2\pi(a-x)}}\left[1+M_1\left(1-\frac{x}{a}\right)^{1/2}+M_2\left(1-\frac{x}{a}\right)^{1}+M_3\left(1-\frac{x}{a}\right)^{3/2}\right] \tag{33}$$

The geometry dependent factors M_1, M_2, and M_3 for an edge and through crack in a finite width plate could be found in the appendix. Additional M_1, M_2, and M_3 factors for various geometrical configurations were given in Refs. [31,32].

The stress intensity factor was calculated by integrating the product of the residual stress $\sigma_r(x)$ and the weight function $m(x,a)$ over the crack surface area.

$$K_r = \int_0^a \sigma_r(x) m(x,a) \mathrm{d}x \tag{34}$$

The physical crack tip location at '$x=a$' was chosen as the upper limit of the integration in the expression (34). It was also found that region r_p was close to the cyclic plastic zone size. A special numerical procedure [33] was developed for calculating the integral (34).

3.4. Calculation of the resultant (total) maximum and minimum stress intensity factors

The residual stress effect cannot be assessed by simple superposition of stress intensity factors because the character of the crack opening displacement field needs to be accounted for. It is shown qualitatively in Fig. 2(f) that the compressive residual stresses might be induced at tensile levels of the minimum load. Further decrease of the applied load below point C (Fig. 2(e) and (f)) reverses the crack tip plastic deformation induced during the preceding reversal. The plastic zone on the other hand resists to be deformed in reverse direction during the unloading process and therefore the crack tip stress–strain path ends at point E (Fig. 2(f)) instead of point E′ what would be the case if the plastic zone did not resist to deformation. In other words, the strain and stress at the crack tip change very little when the load decrease from point D to E. In terms of the stress intensity factor, the plastic zone and the residual stress manifest themselves mainly in a change (increase) of the resultant minimum stress intensity factor $K_{min,tot}$ without significant changes in the resultant maximum stress intensity factor $K_{max,tot}$. It is assumed that the residual stress intensity factor K_r contributes mainly to changes (increases) of the minimum resultant stress intensity factor $K_{min,tot}$ and subsequently the resultant stress range ΔK_{tot}.

Two distinct cases need to be considered while determining the resultant stress intensity factor parameters.

3.4.1. Case 1. $\tilde{\sigma}^a_{min} \geq 0$

At relatively high applied stress ratios ($R_{appl} > 0.5$) the reversed plastic deformations around the crack tip are not sufficient to produce compressive stresses (see Fig. 6(a)). Therefore, the resultant stress intensity factor quantities are determined as follows:

$$K_{min,tot} = K_{min,net} = K_{min,appl} \tag{35}$$

$$K_{max,tot} = K_{max,net} = K_{max,appl} \tag{36}$$

$$\Delta K_{tot} = K_{max,tot} - K_{min,tot} = \Delta K_{net} = \Delta K_{appl} \tag{37}$$

3.4.2. Case 2. $\tilde{\sigma}^a_{min} < 0$

It is known that compressive residual stresses at the notch/crack tip can be generated even at the minimum tensile load if the applied stress ratio is relatively low $R_{appl} < 0.5$. However, the procedure for calculating the resultant stress intensity factor accounting for the effect of residual stresses is different for tensile applied minimum stress intensity factor $K_{min,appl} > 0$ and the compressive minimum stress intensity factor $K_{min,appl} < 0$. The negative stress intensity factor has no physical meaning but is mathematically useful while characterizing the load reversals. The difference between these two cases lies in the calculation procedure concerning the input of the pseudo-elastic net crack tip stresses described in Section 3.1.

The negative residual stress intensity factor K_r has no physical meaning but it reflects the contribution of the residual stress to the resultant minimum stress intensity factor $K_{min,tot}$.

The resultant minimum stress intensity factor $K_{min,tot}$ 'felt' by the material at the crack tip is in such a case equal to the algebraic sum of the minimum net stress intensity factor $K_{min,net}$ and the negative residual SIF, K_r.

$$\begin{aligned} K_{min,tot} &= K_{min,net} - K_r \\ &= K_{min,appl} - K_r \qquad \text{for} \quad K_{min,appl} \geq 0 \\ K_{min,tot} &= K_{min,net} - K_r \\ &= K_{min,appl} \frac{3}{2Y} \sqrt{\frac{\rho^*}{a}} - K_r \quad \text{for} \quad K_{min,appl} < 0 \end{aligned} \tag{38}$$

The resultant maximum stress intensity factor $K_{max,tot}$, as discussed above, is not affected by the compressive residual stress.

$$K_{max,tot} = K_{max,net} = K_{max,appl} \tag{39}$$

The two equations above enable the resultant stress intensity range ΔK_{tot} to be determined in terms of the applied and the residual stress intensity factor.

$$\begin{aligned} &\text{for} \quad K_{min,appl} \geq 0 \\ &\Delta K_{tot} = K_{max,tot} - K_{min,tot} = K_{max,appl} - K_{min,appl} + K_r \\ &\quad = \Delta K_{appl} + K_r \\ &\text{for} \quad K_{min,appl} < 0 \\ &\Delta K_{tot} = K_{max,tot} - K_{min,tot} \\ &\quad = K_{max,appl} - K_{min,appl} \frac{3}{2Y} \sqrt{\frac{\rho^*}{a}} + K_r = \Delta K_{net} + K_r \end{aligned} \tag{40}$$

The resultant maximum SIF, $K_{max,tot}$ and the resultant stress intensity range are two main parameters governing the fatigue crack growth rate. However, they need to be combined into one driving force expression analogously to

the fatigue damage parameter used in the classical fatigue theories.

4. Analytical derivation of the fatigue crack driving force $\Delta\kappa$ and the fatigue crack growth expression $da/dN - \Delta\kappa$

Expressions (14)–(16) and (24–(26) and the Neuber rule provide the link between the stress–strain response at the crack tip and the applied stress intensity factor history. Therefore, the fatigue crack expression can be derived based on selected fatigue damage accumulation parameter and the crack tip stress–strain history.

The Smith–Watson–Topper (SWT) damage parameter [22] was chosen to determine the fatigue damage accumulation at the crack tip.

$$D = \tilde{\sigma}^{a}_{max}\frac{\Delta\tilde{\varepsilon}^{a}}{2} \tag{41}$$

After including the SWT damage parameter into the Manson–Coffin strain–life fatigue curve, the following expression is obtained relating the SWT damage parameter with the number of cycles to failure.

$$\tilde{\sigma}^{a}_{max}\frac{\Delta\tilde{\varepsilon}^{a}}{2} = \frac{(\sigma'_f)^2}{E}(2N_f)^{2b} + \sigma'_f\varepsilon'_f(2N_f)^{b+c} \tag{42}$$

Eqs. (31) and (32) provide unique relationship between the applied SIF and the actual strains and stresses. Unfortunately, these equations only hold true in the case of cracks subjected to cyclic loads applied at relatively high stress ratios $R>0.5$. In the case of low stress ratios, a compressive residual stress field is generated ahead of the crack tip and Eqs. (31) and (32) can be used providing that the net maximum SIF, $K_{max,net}$, and the net SIF range, ΔK_{net}, are corrected for the effect of the residual stress, σ_r. In other words, the resultant maximum SIF, $K_{max,tot}$ and the resultant SIF range, ΔK_{tot} discussed above must be used in these equations.

The actual maximum stress can be obtained from the set of two equations involving the resultant stress intensity factor $K_{max,tot}$ and the cyclic stress–strain material curve.

$$\begin{cases} \dfrac{1}{E}\left(\dfrac{K_{max,tot}\times\psi_{y,1}}{\sqrt{2\pi\rho^*}}\right)^2 = \dfrac{(\tilde{\sigma}^{a}_{max})^2}{E} + \tilde{\sigma}^{a}_{max}\left(\dfrac{\tilde{\sigma}^{a}_{max}}{K'}\right)^{1/n'} \\ \tilde{\varepsilon}^{a}_{max} = \dfrac{\tilde{\sigma}^{a}_{max}}{E} + \left(\dfrac{\tilde{\sigma}^{a}_{max}}{K'}\right)^{1/n'} \end{cases} \tag{43}$$

The actual crack tip strain range can be determined from the set of two equations involving the resultant stress intensity range ΔK_{tot} and the cyclic stress–strain material curve expanded by factor of two.

$$\begin{cases} \dfrac{1}{E}\left(\dfrac{\Delta K_{tot}\times\psi_{y,1}}{\sqrt{2\pi\rho^*}}\right)^2 = \dfrac{(\Delta\tilde{\sigma}^{a})^2}{E} + 2(\Delta\tilde{\sigma}^{a})\left(\dfrac{\Delta\tilde{\sigma}^{a}}{2K'}\right)^{1/n'} \\ \dfrac{\Delta\tilde{\varepsilon}^{a}}{2} = \dfrac{\Delta\tilde{\sigma}^{a}}{2E} + \left(\dfrac{\Delta\tilde{\sigma}^{a}}{2K'}\right)^{1/n'} \end{cases} \tag{44}$$

Unfortunately, closed form solutions for $\tilde{\sigma}^{a}_{max}$ and $\Delta\tilde{\varepsilon}^{a}$ are not feasible. However, approximate closed form solutions are feasible if some terms in Eqs. (43) and (44) are neglected. At high applied loads, i.e. at high maximum stress intensity factors and high stress intensity ranges, the strains at the crack tip are predominantly plastic. Therefore, the elastic terms in Eqs. (43) and (44) can be neglected. In the near threshold fatigue crack growth region, the strains at the crack tip are predominantly elastic and therefore the plastic terms in Eqs. (43) and (44) can be neglected.

—Predominantly plastic behavior of material at the crack tip.

Eqs. (43) and (44) take simpler form after neglecting the elastic terms.

$$\begin{cases} \dfrac{1}{E}\left(\dfrac{K_{max,tot}\times\psi_{y,1}}{\sqrt{2\pi\rho^*}}\right)^2 = \tilde{\sigma}^{a}_{max}\left(\dfrac{\tilde{\sigma}^{a}_{max}}{K'}\right)^{1/n'} \\ \tilde{\varepsilon}^{a}_{max} = \left(\dfrac{\tilde{\sigma}^{a}_{max}}{K'}\right)^{1/n'} \end{cases} \tag{45}$$

$$\begin{cases} \dfrac{1}{E}\left(\dfrac{\Delta K_{tot}\times\psi_{y,1}}{\sqrt{2\pi\rho^*}}\right)^2 = 2(\Delta\tilde{\sigma}^{a})\left(\dfrac{\Delta\tilde{\sigma}^{a}}{2K'}\right)^{1/n'} \\ \dfrac{\Delta\tilde{\varepsilon}^{a}}{2} = \left(\dfrac{\Delta\tilde{\sigma}^{a}}{2K'}\right)^{1/n'} \end{cases} \tag{46}$$

The maximum stress and the strain range at the crack tip can be subsequently determined in a closed form.

$$\begin{cases} \tilde{\sigma}^{a}_{max} = \left(\dfrac{(K')^{1/n'}(\psi_{y,1})^2}{2\pi E\rho^*}\right)^{n'/(n'+1)}(K^2_{max,tot})^{n'/(n'+1)} \\ \Delta\tilde{\varepsilon}^{a} = \left(\dfrac{2^{n'}(\psi_{y,1})^2}{4\pi EK'\rho^*}\right)^{1/(n'+1)}(\Delta K^2_{tot})^{n'/(n'+1)} \end{cases} \tag{47}$$

For consistency reason, the elastic term in the strain–life expression (42) should be neglected as well.

$$\tilde{\sigma}^{a}_{max}\frac{\Delta\tilde{\varepsilon}^{a}}{2} = \sigma'_f\varepsilon'_f(2N_f)^{b+c} \tag{48}$$

After substituting for the maximum stress and the strain range in Eq. (48), one can write the expression relating the number of cycles to failure to the two stress intensity factor parameters.

$$\left(\frac{(\psi_{y,1})^2}{2^{(n'+3)/(n'+1)}\pi E\rho^*}\right)(K^2_{\max,\text{tot}})^{n'/(n'+1)}(\Delta K^2_{\text{tot}})^{1/(n'+1)} = \sigma'_f\varepsilon'_f(2N_f)^{b+c} \tag{49}$$

The number of cycles N_f needed to fail the elementary material block at the crack tip is:

$$N_f = \frac{1}{2}\left[\frac{1}{\sigma'_f\varepsilon'_f}\times\frac{(\psi_{y,1})^2}{2^{(n'+3)/(n'+1)}\pi E\rho^*} \times(K^2_{\max,\text{tot}})^{n'/(n'+1)}(\Delta K^2_{\text{tot}})^{1/(n'+1)}\right]^{1/(b+c)} \tag{50}$$

The fatigue crack growth rate (7) can be subsequently calculated as:

$$\frac{da}{dN} = \frac{\rho^*}{N_f} = 2\rho^*\left[\frac{1}{\sigma'_f\varepsilon'_f}\times\frac{(\psi_{y,1})^2}{2^{(n'+3)/(n'+1)}\pi E\rho^*} \times(K^2_{\max,\text{tot}})^{n'/(n'+1)}(\Delta K^2_{\text{tot}})^{1/(n'+1)}\right]^{-(1/(b+c))} \tag{51}$$

Because the only variables in Eq. (51) are the maximum stress intensity factor and the stress intensity range the fatigue crack growth expression can be written in a short form.

$$\frac{da}{dN} = C[(K_{\max,\text{tot}})^p(\Delta K_{\text{tot}})^{1-p}]^\gamma \tag{52}$$

where

$$C = 2\rho^*\left[\frac{(\psi_{y,1})^2}{2^{(n'+3)/(n'+1)}\sigma'_f\varepsilon'_f\pi E\rho^*}\right]^{-(1/(b+c))}; \quad p = \frac{n'}{n'+1}; \quad \gamma = -\frac{2}{b+c}$$

Eq. (52) indicates how the two stress intensity factor parameters should be combined into one fatigue crack driving force.

—Predominantly elastic behavior of the material at the crack tip

Similar analysis can be carried out for neglected plastic terms in Eqs. (43) and (44) what is believed to be a good approximation of the crack tip material stress–strain behavior in the near threshold fatigue crack growth region. The final fatigue crack growth expression derived for the near threshold fatigue crack growth regime is as follows

$$\frac{da}{dN} = C[(K_{\max,\text{tot}})^p(\Delta K_{\text{tot}})^{1-p}]^\gamma \tag{53}$$

where

$$C = 2\rho^*\left[\frac{(\psi_{y,1})^2}{4\pi\rho^*\sigma'^2_f}\right]^{-1/2b}; \quad p = 0.5; \quad \gamma = -\frac{1}{b}$$

The crack growth expressions (52) and (53) are formally the same as those proposed by Walker [6], Donald and Paris [7] and Kujawski [8] except that the resultant maximum stress intensity factor $K_{\max,\text{tot}}$ and the resultant stress intensity range ΔK_{tot} accounting for the compressive residual stress effect should be applied. The derived crack growth expressions suggest that the fatigue crack driving force accounting for the mean stress effect should be of the form:

$$\Delta\kappa = K^p_{\max,\text{tot}}\Delta K^{1-p}_{\text{tot}} \tag{54}$$

The magnitudes of parameter p indicate that the effect of the maximum stress intensity factor is more significant in the near threshold regime than in the Paris regime of relatively high fatigue crack growth rates.

A similar analysis was also carried out assuming the plane strain state at the crack tip and modifying the stress–strain relationship as proposed in Refs. [34,35]. The form of the fatigue crack driving force (54) derived for the plane strain state at the crack tip was the same as in the case of the uni-axial stress state. The only difference found was the constant C^* in the fatigue crack growth expression.

$$\frac{da}{dN} = C^*[(K_{\max,\text{tot}})^p(\Delta K_{\text{tot}})^{1-p}]^\gamma \tag{55}$$

The constants C^* for the crack tip in plane strain state are:

– for predominantly plastic plane strain behavior of the material at the crack tip

$$C^* = \frac{C}{(1-\nu^2)^{1/(b+c)}} = \frac{2\rho^*}{(1-\nu^2)^{1/(b+c)}}\left[\frac{(\psi_{y,1})^2}{2^{(n'+3)/(n'+1)}\sigma'_f\varepsilon'_f\pi E\rho^*}\right]^{-(1/(b+c))} \tag{56}$$

– for predominantly elastic plane strain behavior of the material at the crack tip

$$C^* = \frac{C}{(1-\nu^2)^{1/2b}} = \frac{2\rho^*}{(1-\nu^2)^{1/2b}}\left[\frac{(\psi_{y,1})^2}{4\pi\rho\sigma'^2_f}\right]^{-1/2b} \tag{57}$$

All constants in the fatigue crack growth expressions derived above are known if the material properties in the form of the cyclic stress–strain curve (4) and the fatigue strain–life expression (5) are available. The only unknown parameter needed to be determined is the size of the elementary material block, ρ^*.

4.1. Determination of the elementary material block size ρ^*

In order to determine the elementary material block size ρ^* some fatigue crack growth data are necessary. The obvious properties are the threshold stress intensity factor ΔK_{th} and the fatigue limit $\Delta\sigma_{th}$. For the fatigue crack not to grow at the threshold stress intensity range ΔK_{th}, the local stress at the crack tip must be equal to the fatigue limit $\Delta\sigma_{th}$. Due to the fact that the fatigue limit is less than the material yield limit the elastic stress–strain analysis can be carried out. Thus, according to the Creager–Paris solution the two material properties can be related as:

$$\Delta\tilde{\sigma}^{a}_{th} = \frac{\Delta K_{th} \times \psi_{y,1}}{\sqrt{2\pi\rho^*}} \tag{58}$$

Eq. (59) may be subsequently used for the determination of the elementary material block size ρ^*.

$$\rho^* = \frac{(\psi_{y,1})^2}{2\pi}\left(\frac{\Delta K_{th}}{\Delta\tilde{\sigma}^{a}_{th}}\right)^2 \tag{59}$$

The elementary material block size (59) is in such a case close to the well-known parameter resulting from the Kitagawa diagram [36]. However, care must be taken in order to use the fatigue limit $\Delta\tilde{\sigma}^{a}_{th}$ obtained at the same stress ratio R as the stress ratio at the crack tip induced by the threshold stress intensity range ΔK_{th}. However, some care needs to be taken while determining the threshold stress intensity factors. Namely, the fatigue crack may not grow because of one of the two reasons [9], i.e. either the applied maximum stress intensity factor is less than the maximum threshold stress intensity factor ($K_{max,appl} < K_{max,th}$) or the applied stress intensity range is less than the threshold stress intensity range ($\Delta K_{appl} < \Delta K_{th}$). If the crack cease to grow at the stress ratio $R=0$ it is not certain whether the maximum stress intensity or the stress intensity range was reached the threshold level. Therefore, the optimum stress ratio at which the threshold stress range ΔK_{th} can be determined without producing significant plasticity at the maximum stress intensity factor is $0.2 < R < 0.3$ and in such a case the 'elastic' solution Eq. (59), can be used.

An alternative method of estimating parameter ρ^* can be used if experimental fatigue crack growth data from near the threshold region is available. If the near threshold fatigue crack growth rate generated at $K_{max,appl}$ and ΔK_{appl} is known the constant C can be determined from Eq. (53).

$$C = \frac{da}{dN}[(K_{max,tot})^p(\Delta K_{tot})^{1-p}]^{-\gamma} \tag{60}$$

The unknown elementary material block size ρ^* can be subsequently determined from the expression for the C constant (see Eq. (53))

$$\rho* = \left\{\frac{C}{2}\left[\frac{(\psi_{y,1})^2}{4\pi(\sigma'_f)^2}\right]^{1/2b}\right\}^{2b/(2b+1)} \tag{61}$$

In order to avoid producing plastic strains and compressive residual stresses near the crack tip it is recommended to use the near threshold fatigue crack growth data obtained at stress ratios $R > 0.5$.

5. Experimental verification

Fatigue crack growth data of three materials were used for the validation of the model. There were one steel 4340 material and two aluminum alloys Al 7075-T6 and Al 2024-T351. The cyclic (4) and fatigue properties (5) for each material are given in Table 1.

5.1. Modeling of fatigue crack growth 4340 steel material

The fatigue crack growth data for the 4340 steel material was found in Refs. [37,38]. The fatigue crack growth data sets obtained at various stress ratios R_{appl} are shown in Fig. 7 as a function of the applied stress intensity range ΔK_{appl}.

Table 1
Material properties

		Material		
		Al 7075-T6	Al 2024-351	St-4340
Monotonic material properties	E (MPa)	71,000	70,000	200,000
	ν	0.32	0.32	0.3
	σ_{ys} (MPa)	468.85	403.46	889.32
Cyclic stress–strain curve	K' (MPa)	780.64	751.1	1910
	n'	0.088	0.1	0.123
Strain–life curve	σ'_f (MPa)	780.64	737.7	1879
	b	−0.045	−0.081	−0.0895
	ε'_f	0.19	0.3/0.066[a]	0.64
	c	−0.52	−0.6/−0.35[a]	−0.636
Near threshold FCG data	da/dN (mm/cycle)	5×10^{-8} at $R=0.5$	6×10^{-7} at $R=0.3$	1×10^{-7} at $R=0.7$
	$\Delta\kappa$ (MPa$\sqrt{m}$)	1.98 at $R=0.5$	2.68 at $R=0.3$	4.56 at $R=0.7$
Crack tip radius	ρ^* (m)	4.03×10^{-6}	1.6×10^{-5}	1.1×10^{-5}

[a] The fatigue strain–life curve (5) was approximated by two linear segments in the log–log co-ordinates. The two lines intersect at $2N_f = 420$ cycles (or strain amplitude $\Delta\varepsilon/2 = 0.008$).

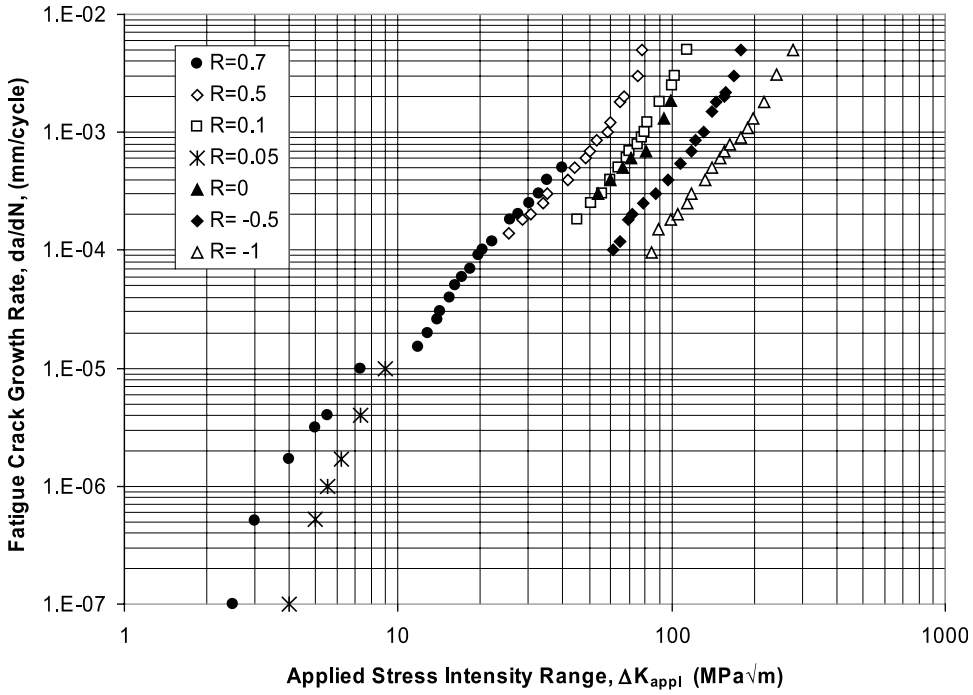

Fig. 7. Fatigue crack growth data for 4340 steel obtained at stress ratios $-1 \leq R \leq 0.7$.

The cyclic (4) and fatigue properties (5) for the 4340 steel were borrowed from Refs. [37,39] and they are listed in Table 1. The near threshold fatigue crack growth rate da/dN data obtained at the stress ratio $R=0.7$, shown in Table 1, was selected for the determination of the ρ^* parameter from Eq. (61). Based on the material data listed in Table 1 and the ρ^* parameter, the following constants were obtained for Eqs. (52) and (53):

–for predominantly plastic strain–stress behavior at the crack tip, Eq. (52).

$C=2.36\times10^{-11}$, $p=0.11$, $\gamma=2.76$ (for da/dN in 'mm/cycle' and K in 'MPa$\sqrt{\text{m}}$')

–for predominantly elastic strain–stress behavior at the crack tip, Eq. (53).

$C=5.05\times10^{-18}$, $p=0.5$, $\gamma=11.17$ (for da/dN in 'mm/cycle' and K in 'MPa$\sqrt{\text{m}}$').

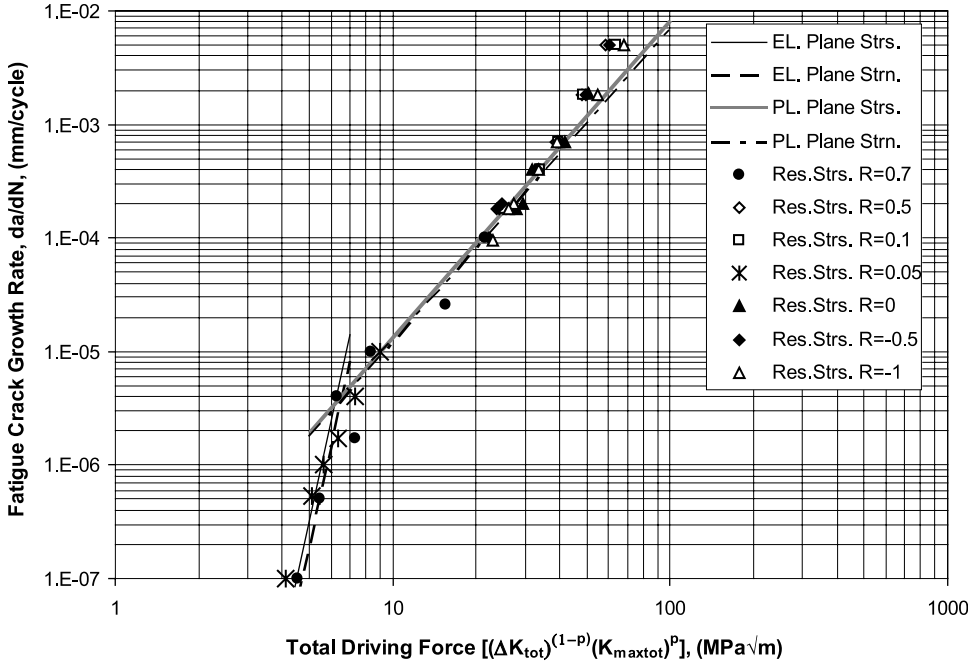

Fig. 8. Fatigue crack growth data for 4340 steel as a function of the two parameter driving force, $\Delta\kappa$.

The fatigue crack growth Eqs. (52) and (53) are shown as lines in the log–log coordinates in Fig. 8. In addition, the fatigue crack growth expressions derived for the plane strain state (Eqs. (55)–(57)) have been plotted. All experimental fatigue crack growth data sets are also shown in the same figure as a function of the driving force $\Delta\kappa$, Eq. (54). The resultant stress intensity factors corrected for the residual stress effect were used to determine the magnitude of the driving force $\Delta\kappa$. It is seen that both fatigue crack expressions (52) and (53) consolidate well the entire set of fatigue crack growth data obtained at various stress ratios in the range of $-1 < R_{\text{appl}} < 0.7$.

5.2. Modeling of fatigue crack growth in Al 7075-T6 alloy

The fatigue crack growth data for Al 7075-T6 alloy was found in Ref. [40] and used for the comparisons. The fatigue crack growth data sets obtained at various stress ratios R_{appl} are shown in Fig. 9 as a function of the applied stress intensity range ΔK_{appl}.

The cyclic (4) and fatigue properties (5) of the Al 7075-T6 alloy were borrowed from Ref. [13]. Similar data concerning the Al 7075-T6 alloy can also be found on the Society of Automotive Engineers (SAE) web site (fde.uwaterloo.ca) maintained by the Fatigue Design and Evaluation Committee. All necessary parameters of the cyclic stress–strain and the fatigue strain–life curves are listed in Table 1. The fatigue crack growth rate, da/dN obtained at the stress ratio $R=0.5$ and Eq. (61) were selected for the determination of parameter ρ^* and shown in Table 1. Based on the material data listed in Table 1, the following parameters for the crack growth Eqs. (52) and (53) were determined:

–for predominantly plastic material behavior at the crack tip, Eq. (52).

$C=2.45\times10^{-10}$, $p=0.081$, $\gamma=3.54$ (for da/dN in 'mm/cycle' and K in 'MPa$\sqrt{\text{m}}$')

–for predominantly elastic material behavior at the crack tip—Eq. (53)

$C=1.32\times10^{-17}$, $p=0.5$, $\gamma=22.7$ (for da/dN in 'mm/cycle' and K in 'MPa$\sqrt{\text{m}}$')

The fatigue crack growth, Eqs. (52) and (53) are shown in Fig. 10 as solid lines in the log–log coordinates. In addition, the fatigue crack growth expressions derived for the plane strain state (Eqs. (55)–(57)) have been plotted. All experimental fatigue crack growth data sets are also shown in the same figure as a function of the same driving force $\Delta\kappa$, Eq. (54). The resultant stress intensity factors corrected for the compressive residual stress effect were used to determine the magnitude of the driving force $\Delta\kappa$. It is seen that both fatigue crack expressions (52) and (53) consolidate well all fatigue crack growth data obtained at various stress ratios in the range of $-1 < R_{\text{appl}} < 0.5$.

5.3. Modeling of fatigue crack growth in Al 2024-T351 alloy

The fatigue crack growth data for Al 2024-T351 alloy obtained at stress ratios $-1 < R < 0.5$ were borrowed from Ref. [41]. The fatigue crack growth data set obtained at stress ratio $R=-2$ was found in Ref. [42]. All fatigue crack growth data sets are shown in Fig. 11 as a function of the applied stress intensity range ΔK_{appl}.

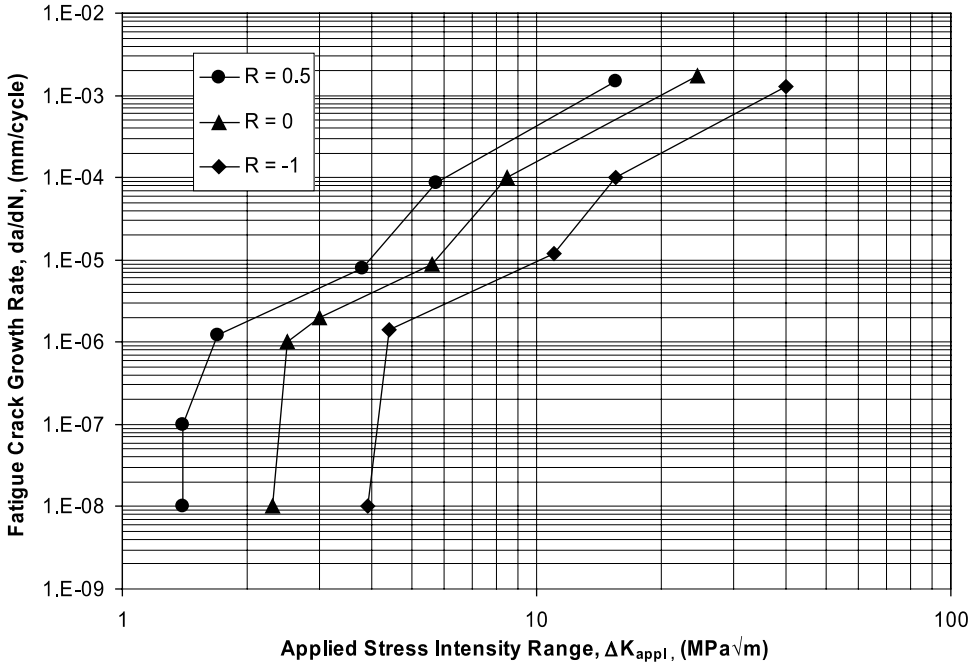

Fig. 9. Fatigue crack growth data for Al 7075-T6 aluminium alloy obtained at stress ratios $-1 \le R \le 0.5$.

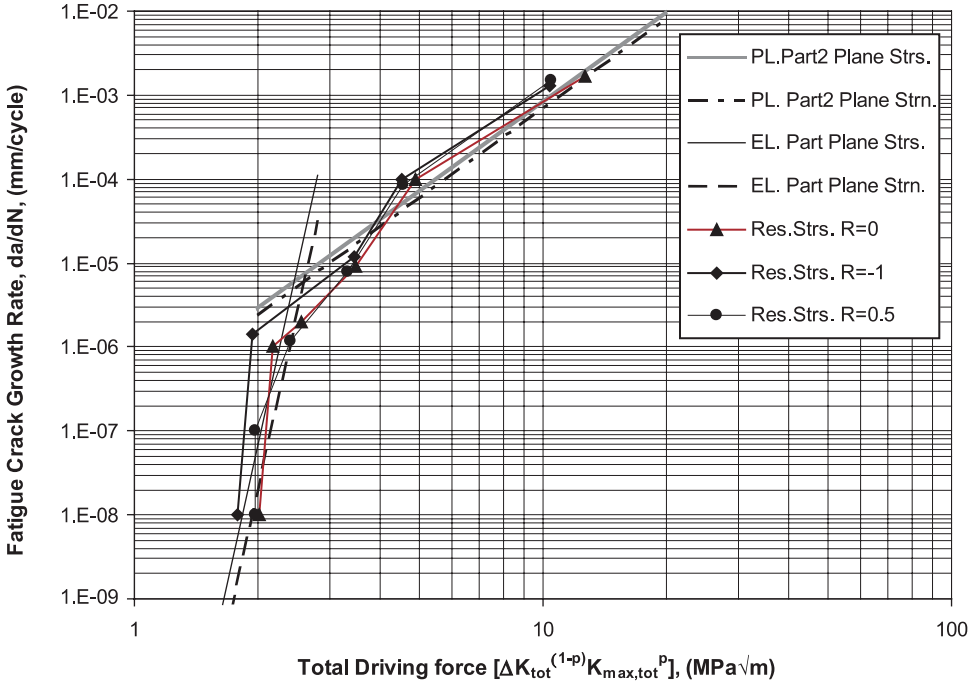

Fig. 10. Fatigue crack growth data for Al 7075-T6 aluminium alloy as a function of the two parameter driving force, $\Delta\kappa$.

The cyclic (4) and fatigue properties (5) of the Al 2024-T351 alloy were borrowed from Ref. [43] but the same data can also be found on the Society of Automotive Engineers (SAE) web site (fde.uwaterloo.ca) maintained by the Fatigue Design and Evaluation Committee. Because the experimental data points concerning the fatigue strain–life data could not be sufficiently well fitted into one Manson–Coffin strain–life curve, two curves were fitted and two sets of parameters were used as shown in Table 1. The fatigue crack growth rate, da/dN obtained at the stress ratio $R=0.3$ and Eq. (61) were selected for the determination of parameter ρ^* and shown in Table 1. Based on the material data listed in Table 1, the following parameters for the crack growth Eqs. (52) and (53) were determined:

–for predominantly plastic material behavior at the crack tip, Eq. (52)

$C=2.74\times10^{-10}$, $p=0.091$, $\gamma=3.09$ and $C=7.79\times10^{-12}$, $p=0.091$, $\gamma=5.19$ (for da/dN in 'mm/cycle' and K in 'MPa$\sqrt{\text{m}}$')

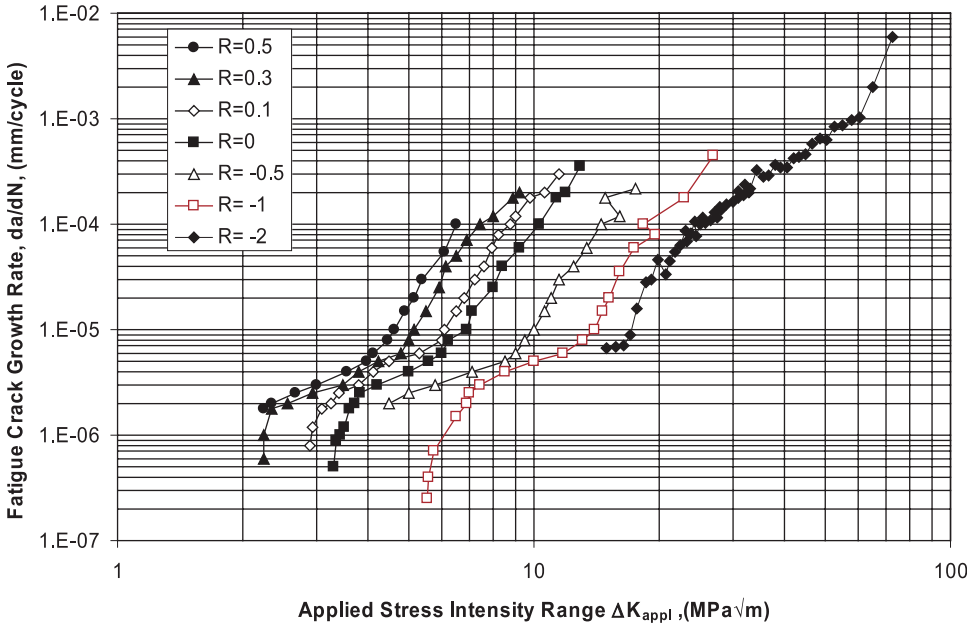

Fig. 11. Fatigue crack growth data for Al 2024 T351 aluminium alloy obtained at stress ratios $-2\leq R\leq0.5$.

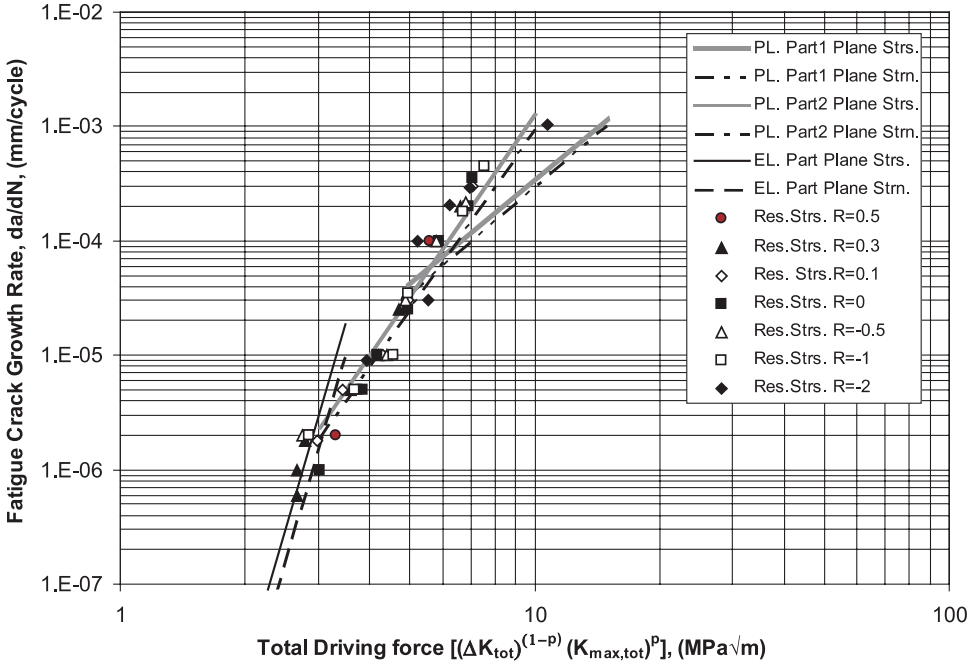

Fig. 12. Fatigue crack growth data for Al 2024 T351 aluminium alloy as a function of the two parameter driving force, $\Delta\kappa$.

–for predominantly elastic material behavior at the crack tip, Eq. (53)

$C=3.56\times10^{-15}$, $p=0.5$, $\gamma=12.35$ (for da/dN in 'mm/cycle' and K in 'MPa$\sqrt{\text{m}}$').

The fatigue crack growth Eqs. (52) and (53) are shown as solid lines in the log–log coordinates in Fig. 12. The fatigue crack growth expressions derived for the plane strain state (Eqs. (55)–(57)) are plotted as dashed lines. It was found that only the expression (52) obtained on the basis of the Manson–Coffin strain–life curve fitted into the high strain (short lives) fatigue data points coincided well with the experimental fatigue crack growth data. The Manson–Coffin expression fitted into the low strain (high life) experimental data points did not provide good data for the fatigue crack growth modeling. The resultant stress intensity factors corrected for the residual stress effect were used to determine the magnitude of the driving force $\Delta\kappa$. It is seen that both fatigue crack expressions (52) and (53) consolidate well fatigue crack growth data obtained at various stress ratios from the stress ratio range of $-2<R_{\text{appl}}<0.5$. It has been also found that in the case of aluminum alloys fitting one Manson–Coffin curve into the low and high cycle fatigue data is inaccurate and two Manson–Coffin curves having two different slopes are recommended.

6. Conclusions

A fatigue crack growth model based on the analysis of elastic–plastic stress–strain history at the crack tip was proposed. It was assumed that the crack can be modeled as a long notch with the tip radius ρ^*. The entire analysis was carried out as for classical notch without the necessity of introducing the concept of the crack closure behind the crack tip. It was found that the simulated crack tip stress–strain history and the Smith–Watson–Topper fatigue damage parameter made it possible to derive fatigue crack growth expressions analogous to previously proposed fatigue crack growth equations accounting for the mean stress effect. The inclusion of the residual stress effect into the fatigue crack growth driving force made it possible to derive one fatigue crack growth expression valid for a wide variety of loading conditions with stress ratios in the range of $-2<R<0.7$. It is also possible to predict the fatigue crack growth rate based on the Ramberg–Osgood stress–strain material curve and the fatigue strain–life Manson–Coffin equation obtained from smooth material specimens tested under constant amplitude strain control loading. It has been noticed that in the case of aluminum alloy Al 2024-T351, the two regions of the high fatigue crack growth data (Paris regime) showing distinctly two different slopes on the da/d$N-\Delta\kappa$ plot coincide with different slopes of the two segment Manson–Coffin curve corresponding to the low and high cycle fatigue data.

The Creager–Paris solution used in the analysis is only valid for long cracks ($a\gg\rho^*$); therefore it would be inaccurate for short cracks whose lengths are comparable with the elementary material block size ρ^*. In the latest case the standard notch stress–strain analysis should be used making the model potentially capable of addressing the short crack problems as well.

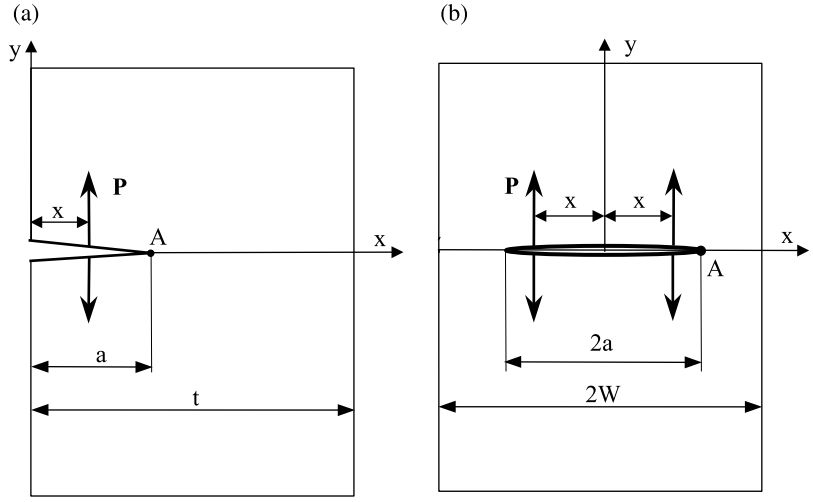

Fig. 13. The system of coordinates and nomenclature for the universal weight function: (a) edge crack in a finite width plate; (b) through central crack in a finite width plate.

Appendix

Parameters $M1$, $M2$, and $M3$ for an edge crack in a finite width plate. See Fig. 13(a) for the nomenclature.

$$M_1 = \frac{-0.029207 + \frac{a}{w}\left(0.213074 + \frac{a}{w}\left(-3.029553 + \frac{a}{w}\left(5.901933 + \frac{a}{w}(-2.657820)\right)\right)\right)}{1.0 + \frac{a}{w}\left(-1.259723 + \frac{a}{w}\left(-0.048475 + \frac{a}{w}\left(0.481250 + \frac{a}{w}\left(-0.526796 + \frac{a}{w}(0.345012)\right)\right)\right)\right)}$$

$$M_2 = \frac{0.451116 + \frac{a}{w}\left(3.462425 + \frac{a}{w}\left(-1.078459 + \frac{a}{t}\left(3.558573 + \frac{a}{t}(-7.553533)\right)\right)\right)}{1.0 + \frac{a}{w}\left(-1.496612 + \frac{a}{w}\left(0.764586 + \frac{a}{w}\left(-0.659316 + \frac{a}{w}\left(0.258506 + \frac{a}{w}(0.114568)\right)\right)\right)\right)}$$

$$M_3 = \frac{0.427195 + \frac{a}{w}\left(-3.730114 + \frac{a}{w}\left(16.276333 + \frac{a}{w}\left(-18.799956 + \frac{a}{w}(14.112118)\right)\right)\right)}{1.0 + \frac{a}{w}\left(-1.129189 + \frac{a}{w}\left(0.033758 + \frac{a}{w}\left(0.192114 + \frac{a}{w}\left(-0.658242 + \frac{a}{w}(0.554666)\right)\right)\right)\right)}$$

Parameters M_1, M_2, and M_3 for a central through crack in a finite width plate subjected to symmetric loading. See Fig. 13(b) for the nomenclature.

$$M_1 = 0.06987 + 0.40117\left(\frac{a}{W}\right) - 5.5407\left(\frac{a}{W}\right)^2 + 50.0886\left(\frac{a}{W}\right)^3 - 200.699\left(\frac{a}{W}\right)^4 + 395.552\left(\frac{a}{W}\right)^5 - 377.939\left(\frac{a}{W}\right)^6 + 140.218\left(\frac{a}{W}\right)^7$$

$$M_2 = -0.09049 - 2.14886\left(\frac{a}{W}\right) + 22.5325\left(\frac{a}{W}\right)^2 - 89.6553\left(\frac{a}{W}\right)^3 + 210.599\left(\frac{a}{W}\right)^4 - 239.445\left(\frac{a}{W}\right)^5 + 111.128\left(\frac{a}{W}\right)^6$$

$$M_3 = 0.427216 + 2.56001\left(\frac{a}{W}\right) - 29.6349\left(\frac{a}{W}\right)^2 + 138.40\left(\frac{a}{W}\right)^3 - 347.255\left(\frac{a}{W}\right)^4 + 457.128\left(\frac{a}{W}\right)^5 - 295.882\left(\frac{a}{W}\right)^6 + 68.1575\left(\frac{a}{W}\right)^7$$

References

[1] Paris PC, Erdogan F. A critical analysis of crack propagation laws. Trans ASME, J Basic Eng 1963;D85:528–34.
[2] Elber W. The significance of fatigue crack closure. In: Damage tolerance in aircraft structure. ASTM STP 486, Philadelphia: American Society for Testing and Materials; 1971; p. 230–42.
[3] Aliaga D, Davy A, Schaff H. A simple crack closure model for predicting fatigue crack growth under flight simulation loading. In: Newman JC, Elber W, editors. Mechanics of fatigue crack closure, ASTM STP 982. Philadelphia: American Society for Testing and Materials; 1988. p. 491–504.

[4] De Köning AU. A simple crack closure model for prediction of fatigue crack growth rates under variable-amplitude loading. In: Roberts R, editor. Fracture mechanics, ASTM STP 743. Philadelphia: American Society for Testing and Materials; 1981. p. 63–85.
[5] Newman JR. Prediction fatigue crack growth under variable-amplitude and spectrum loading using a closure model. In: Abelkis PR, Hudson CM, editors. Design of fatigue and fracture resistant structure, ASTM STP 761. Philadelphia: American Society for Testing and Materials; 1982. p. 255–77.
[6] Walker EK. The effect of stress ratio during crack propagation and fatigue for 2024-T3 and 7076-T6 aluminum. In: Effect of environment and complex load history on fatigue life, ASTM STP 462. Philadelphia: American Society for Testing and Materials; 1970. p. 1–14.
[7] Donald K, Paris PC. An evaluation of ΔK_{eff} estimation procedure on 6061-T6 and 2024-T3 aluminium alloys. Int J Fatigue 1999;21: S47–S57.
[8] Dinda S, Kujawski D. Correlation and prediction of fatigue crack growth for different R-ratios using K_{max} and ΔK^{+} parameters. Eng Fract Mech 2004;71:1779–90.
[9] Vasudevan AK, Sadananda K, Louat N. A review of crack closure, fatigue crack threshold and related phenomena. Mater Sci Eng 1994; A188:1–22.
[10] Irwin GR. Analysis of stresses and strains near the end of a crack traversing a plate. Trans ASME, J Appl Mech 1957;E24:361–4.
[11] Hutchinson JW. Singular behaviour at the end of a tensile crack in a hardening material. J Mech Phys Solids 1968;16:13–31.
[12] Lal DN, Weiss V. A notch analysis of fracture approach to fatigue crack propagation. Metall Trans 1978;9A:413–20.
[13] Kaisand LR, Mowbray DF. Relationships between low-cycle fatigue and fatigue crack growth-rate properties. J Test Eval 1979;7(5): 270–80.
[14] Glinka G. A notch stress-strain analysis approach to fatigue crack growth. Eng Fract Mech 1985;21(2):245–6.
[15] Neuber H. Kerbspannugslehre. Berlin: Springer; 1985.
[16] Jones R. Private communications. DSTO Centre for Structural Mechanics, Department of Mechanical Engineering, Monash University, Victoria, 3800, Australia.
[17] Pommier S. A study of the relationship between variable level fatigue crack growth and the cyclic constitutive behaviour of steel. Int J Fatigue 2001;23:S111–S8.
[18] Sander M, Richard HA. Lifetime prediction for real loading situations—concepts and experimental results of fatigue crack growth. Int J Fatigue 2003;25:999–1005.
[19] Forsyth PJE. Unified description of micro and macroscopic fatigue crack behaviour. Int J Fract 1983;5:3–14.
[20] Landgraf RW, Morrow J, Endo T. Determination of the cyclic stress–strain curve. J Mater 1969;4(1):176.
[21] Technical report on low cycle fatigue properties: ferrous and non-ferrous metals. SAE Standard No. J1099, Society of Automotive Engineers (SAE), Warrendale, Pennsylvania, 1998.
[22] Smith KN, Watson P, Topper TH. A stress–strain function for the fatigue of metals. J Mater 1970;5(4):767–78.
[23] Neuber H. Theory of stress concentration for shear-strained prismatic bodies with arbitrary nonlinear stress–strain law. ASME J Appl Mech 1961;28:544–51.
[24] Creager M, Paris PC. Elastic field equations for blunt cracks with reference to stress corrosion cracking. Int J Fract Mech 1967;3: 247–52.
[25] Moftakhar A, Buczynski A, Glinka G. Calculation of elastoplastic strains and stresses in notched under multiaxial loading. Int J Fract 1995;70(3):337–57.
[26] Glinka G, Buczynski A. Multiaxial stress–strain notch analysis. In: Kalluri S, et al, editors. Multiaxial fatigue and deformation, ASTM STP 1387. Philadelphia: American Society for Testing and Materials; 2000. p. 82–98.
[27] Skrzypek JJ, Hetnarski RB. Plasticity and creep: theory, examples and problems. Boca Raton: CRC Press; 1993.
[28] Burdekin FM, Stone DEW. The crack opening displacement approach to fracture mechanics in yielding materials. J Strain Anal 1966;1: 145–53.
[29] Bueckner HF. A novel principle for the computation of stress intensity factors. Zeitschrift Angewandte Mathematik und Mechanik 1970;50: 529–46.
[30] Glinka G, Shen G. Universal features of weight functions for cracks in mode I. Eng Fract Mech 1991;40(6):1135–46.
[31] Shen G, Glinka G. Determination of weight functions from reference stress intensity factor. Theor Appl Fract Mech 1991;15(3):237–45.
[32] Wang X, Lambert S, Glinka G. Approximate weight functions for embedded elliptical cracks. Eng Fract Mech 1998;59(3):381–92.
[33] Moftakhar A, Glinka G. Calculation of stress intensity factors by efficient integration of weight functions. Eng Fract Mech 1992;43(5):749–56.
[34] Glinka G, Ott W, Nowack H. Elastoplastic plane strain analysis of stresses and strains at the notch root. J Eng Mater Tech 1988;110(3): 195–204.
[35] Nie H, Shaobo L. Biaxial stress fatigue life prediction by the local strain method. Int J Fatigue 1997;19(6):517–22.
[36] Kitagawa H, Takahashi S. Applicability of fracture mechanics to very small cracks in the early stage. In: Processing of the Second International Conference on Mechanical Behaviour of Materials, Metals Park, American Society for Metals, 1976 p. 627–631.
[37] Dowling NE. Mechanical behaviour of materials. New Jersey: Prentice Hall; 1999.
[38] Taylor D. A compendium of fatigue threshold and growth. 1985.
[39] Chen WC, Lawrence FV. A model for joining the fatigue crack initiation and propagation analyses. FCP Report No. 32, University of Illinois at Urbana Champaign - College of Engineering, 1979.
[40] Newman J. Wu XR, Venneri SL, Li CG. Small-crack effects in high-strength aluminium alloys. NASA/CAE Cooperative Program, Report No. NASA RP-1309, Langley Research Center, Hapton VA, 1994.
[41] Pang C-M, Song J-H. Crack growth and closure behaviour of short fatigue cracks. Eng Fract Mech 1994;47(3):327–43.
[42] Liu AF. Structural life assessment methods. Materials Park, OH, USA: ASM International; 1998.
[43] Leis B. Cyclic inelastic deformation behaviour of thin notched plates. Master Thesis, University of Waterloo, Department of Civil Engineering, 1972.